CAUCHY – Jurnal Matematika Murni dan Aplikasi
Volume 11 (1) (2026), Pages 1095-1121
p-ISSN: 2086-0382; e-ISSN: 2477-3344

# Stability and Bifurcation of an Eco-Epidemiological Predator-Prey Model with Harvesting and Migration

Muhammad Thariq Firmansyah and Dian Savitri*

*Department of Mathematics, Universitas Negeri Surabaya, Indonesia*

**Abstract**

This study develops and analyzes a predator-prey eco-epidemiological model incorporating three simultaneous ecological factors: disease in the prey population, constant predator harvesting, and a density-dependent migration-relaxation term $m(x_e - x)$ for healthy prey within a closed ecosystem. The model is formulated as a system of three autonomous ordinary differential equations. Five biologically distinct equilibrium points are identified, ranging from total extinction to full coexistence; a sixth candidate is degenerate. Local stability of each equilibrium is analyzed by Jacobian linearization, with the Routh–Hurwitz criterion applied to the interior coexistence equilibrium $E_6$. A key structural finding is that the migration parameter $m$ does not alter equilibrium locations but appears in the Jacobian, thereby modifying the eigenvalues and accelerating convergence to equilibrium. Bifurcation analysis with respect to the predation rate on infected prey $\varepsilon$ reveals a supercritical Hopf bifurcation at $\varepsilon_H = 0.221$ and a transcritical bifurcation at $\varepsilon_{BP} = 2.501$, partitioning the parameter space into three dynamical regimes: oscillatory coexistence, stable three-species coexistence, and disease eradication. Numerical simulations verify all analytical results. This work extends the model of Mansur et al. [1] by incorporating prey redistribution and a full bifurcation analysis, offering a more complete framework for ecosystems where disease, harvesting, and prey migration co-occur.

**Keywords:** predator-prey model; eco-epidemiology; disease in prey; predator harvesting; migration-relaxation term; local stability; Hopf bifurcation; transcritical bifurcation; Routh–Hurwitz criterion

Copyright © 2026 by Authors, Published by CAUCHY Group. This is an open access article under the CC BY-SA License (https://creativecommons.org/licenses/by-sa/4.0)

## 1. Introduction

Mathematical modeling is one of the branches of applied mathematics that bridges real-world phenomena with abstract representations in the form of mathematical equations [2, 3]. Through this approach, complex problems encountered in nature can be systematically simplified and analyzed, enabling predictions of a system's behavior over time. One field that extensively employs mathematical modeling is ecology, particularly in studying the interactions among organism populations within an ecosystem [4–6].

In ecology, the food chain describes the flow of energy from one organism to another. The most fundamental component of this chain is the predator-prey relationship, in which the survival of a predator population is critically dependent on the availability of its prey. The predator-prey

*Corresponding author. E-mail: diansavitri@unesa.ac.id

Submitted: March 12, 2026 Reviewed: March 28, 2026 Accepted: April 28, 2026
DOI: https://doi.org/10.18860/cauchy.v11i1.41546

model was first introduced independently by Lotka [2] and Volterra [3], whose classical framework assumed that both populations are entirely healthy, so that neither the predator's ability to hunt nor the prey's capacity to escape is hindered by disease. In this model, the densities of prey and predator populations mutually influence each other in a dynamic oscillatory manner, constrained by environmental carrying capacity.

In reality, however, the assumption that the entire prey population is uniformly healthy does not always hold. In natural ecosystems, prey populations can be divided into two subgroups: healthy individuals and those infected by disease. These two groups differ significantly in their ecological characteristics, as healthy prey possess superior escape ability and physical resilience compared to diseased prey, resulting in different predation rates for each group [7–10]. Mansur et al. [1] addressed this biological reality by developing a predator-prey model that incorporates disease within the prey population together with harvesting of the predator, yielding five equilibrium points that describe various possible ecosystem conditions ranging from total extinction to full coexistence of all populations. Further studies have extended eco-epidemiological frameworks by incorporating additional complexity such as prey refuge [9, 11], cooperative hunting [6, 8, 12], fear effects [7, 12, 13], and harvesting strategies [14–16].

Beyond disease and harvesting, another ecologically significant factor often neglected in many models is population migration. Kant and Kumar [17] affirmed that the movement of populations across spatial regions is a universal demographic event occurring in nearly all types of organisms, including mammals, fish, birds, insects, and crustaceans. Dai et al. [18] further demonstrated that seasonal migration of prey between breeding and non-breeding regions can significantly affect population survival, even determining whether a species persists or goes extinct in a given ecosystem. Roy and Roy [15] likewise showed that incorporating migration and harvesting in a drainage-system predator-prey model produces richer dynamical behavior and more ecologically meaningful equilibria. These findings collectively reveal a persistent gap in the literature: most existing predator-prey models that combine disease and harvesting do not simultaneously account for internal prey migration within a closed ecosystem.

The present study addresses this gap by constructing a mathematical model of a predator-prey system that jointly incorporates disease in the prey, harvesting of the predator, and internal migration of healthy prey within a closed ecosystem. Specifically, this research aims to:

1. formulate the mathematical model with these three interacting components;
2. determine the equilibrium points of the model;
3. analyze the local stability of each equilibrium point;
4. verify the analytical results through numerical simulation.

The primary novelty of this work lies in the integration of a density-dependent relaxation term $m(x_e - x)$ into a predator-prey framework that already contains disease-structured prey and predator harvesting [1, 17, 18]. This term is motivated by the ecology of closed ecosystems in which healthy prey redistribute locally in response to density gradients, without permanent emigration from the system. It is important to note that this formulation does not constitute an explicit multi-patch or spatial model: the system remains a three-dimensional ODE, and the relaxation term is best understood as a phenomenological description of density-dependent redistribution rather than a full spatial conservation law. Unlike external migration models [15, 16, 19], no individual permanently leaves or enters the system, and the total population is subject to the usual demographic processes of growth, disease mortality, natural mortality, and predator harvesting. The key structural effect of the relaxation term is that it modifies the $(1, 1)$ entry of the Jacobian without altering any equilibrium coordinate, thereby influencing the eigenvalues and the rate at which the system recovers from perturbations. This effect is made analytically transparent through eigenvalue analysis. The model thus extends the work of Mansur et al. [1] by incorporating a prey redistribution mechanism and a full bifurcation analysis, offering a more complete dynamical picture of ecosystems where disease, harvesting, and local prey movement

co-occur [15, 17, 18].

The remainder of this paper is organized as follows. Section 2 presents the mathematical formulation of the model, including variable definitions, parameter descriptions, underlying biological assumptions, and the complete analytical framework comprising equilibrium analysis and local stability conditions. Section 3 presents numerical simulations to verify the analytical results and discusses their ecological implications. Finally, Section 4 summarizes the main findings and outlines directions for future work.

## 2. Methods

This section presents the complete mathematical framework of the proposed model. The analysis follows a standard sequence that begins with model construction and ends with stability criteria, mirroring the approach adopted in related eco-epidemiological studies [1, 17]. First, the model equations are derived from biological assumptions and the state variables and parameters are defined. Second, the positivity and boundedness of solutions are established to confirm biological validity. Third, the equilibrium points are determined by solving the algebraic system obtained by setting all time derivatives to zero. Fourth, the local stability of each equilibrium is examined through linearization, whereby the Jacobian matrix is evaluated at each equilibrium and either the eigenvalues are computed directly or the Routh–Hurwitz criterion is applied.

### 2.1. Model Formulation

The model developed in this study represents a closed predator-prey ecosystem structured into three population compartments whose densities evolve continuously over time. The three state variables are $x(t)$, the density of healthy (susceptible) prey at time $t$; $y(t)$, the density of infected prey at time $t$; and $p(t)$, the density of the predator population at time $t$. Healthy prey are individuals that have not been exposed to disease and are capable of natural growth; their local density is subject to a relaxation tendency toward a reference level $x_e$ that phenomenologically represents density-dependent redistribution within the habitat. Infected prey are individuals that have contracted disease through contact with other infected prey. This compartment has no recovery pathway, so the only way out is death, whether from disease or predation. The predator shares the same habitat as both prey groups, derives energy from both, but its population is subject to external harvesting pressure.

The model is constructed as an extension of the work of Mansur et al. [1], which formulated a predator-prey system with disease in the prey and constant harvesting of the predator. The present model retains that framework and introduces an additional term representing the internal migration of healthy prey within the closed ecosystem, motivated by the spatial dynamics studied by Kant and Kumar [17] and Dai et al. [18]. The disease transmission mechanism follows the law of mass action as adopted in [1, 17], predation on healthy prey follows a linear (Holling Type I) functional response, and predation on infected prey likewise follows a linear rate, consistent with the formulation in [1]. All parameters in the model are assumed to be positive constants. Their biological interpretations are summarized in Table 1.

The model is built on the following biological assumptions, established to maintain ecological realism while preserving mathematical tractability. In the absence of disease and predator, healthy prey grow logistically with intrinsic growth rate $r$ and carrying capacity $K$, reflecting the finite resource availability of the environment [1, 17]. Disease transmission occurs exclusively within the prey population through direct contact between healthy and infected individuals, with intensity proportional to the product of their densities (law of mass action); the predator is not susceptible to the disease even when consuming infected prey [1, 5]. Infected prey receive no treatment and cannot recover, so $y$ can only decrease through natural death, disease-induced mortality, or predation [1].

The predator's consumption of both prey types follows a linear functional response, meaning the predation rate scales directly with prey density without saturation, an assumption that keeps

**Table 1:** Definition of model parameters

| Symbol | Biological meaning |
|---|---|
| $r$ | Intrinsic growth rate of healthy prey |
| $K$ | Environmental carrying capacity of healthy prey |
| $\beta$ | Disease transmission rate (contact rate between healthy and infected prey) |
| $\alpha$ | Predation rate of predator on healthy prey |
| $\varepsilon$ | Predation rate of predator on infected prey |
| $\mu_1$ | Natural mortality rate of healthy prey |
| $\mu_2$ | Natural mortality rate of infected prey |
| $\mu_3$ | Natural mortality rate of predator |
| $\delta$ | Additional disease-induced mortality rate of infected prey |
| $h$ | Harvesting rate of predator by external factors |
| $a$ | Conversion coefficient from healthy prey to predator biomass |
| $b$ | Conversion coefficient from infected prey to predator biomass |
| $m$ | Internal migration rate of healthy prey across spatial patches |
| $x_e$ | Reference density of healthy prey used as the migration equilibrium target |

the system analytically tractable and is consistent with the baseline formulation in [1]. Harvesting of the predator occurs at a constant proportional rate $h$, representing external pressure such as human hunting or trapping, following the approach of [1, 15]. The ecosystem is closed in the sense that no individual permanently emigrates from or immigrates into the system, although total population size is not conserved because the model includes logistic growth, disease mortality, natural mortality, and harvesting.

The local redistribution of healthy prey is captured by a single density-dependent relaxation term $m(x_e - x)$ in the $x$-equation. When local density $x$ falls below the reference level $x_e$ an inflow effect occurs, and when $x$ exceeds $x_e$ an outflow effect occurs, driving the healthy prey density toward the reference level $x_e$. This term is a phenomenological one-compartment approximation of prey redistribution; it does not arise from a multi-patch spatial conservation law, and therefore $x_e$ is best interpreted as a model parameter representing the density toward which local redistribution is directed. At any equilibrium of the system, the condition $dx/dt = 0$ requires the migration flux to vanish, which implies $x^* = x_e$ at each equilibrium. Consequently, the relaxation term does not alter the location of any equilibrium point, but it appears in the $(1, 1)$ entry of the Jacobian matrix and therefore directly affects the eigenvalues governing the rate of convergence toward equilibrium [17, 18].

Based on these variables, parameters, and assumptions, the dynamics of the three population compartments are described by the following system of nonlinear autonomous ordinary differential equations:

$$\frac{dx}{dt} = rx\left(1 - \frac{x}{K}\right) - \beta xy - \alpha xp - \mu_1 x + m(x_e - x), \tag{1}$$

$$\frac{dy}{dt} = \beta xy - \varepsilon yp - \mu_2 y - \delta y, \tag{2}$$

$$\frac{dp}{dt} = axp + byp - \mu_3 p - hp. \tag{3}$$

The system in Eqs. (1)–(3) is subject to initial conditions $x(0) = x_0 > 0$, $y(0) = y_0 \geq 0$, and $p(0) = p_0 \geq 0$. Since all parameters are positive and all initial conditions are non-negative, the solutions of the system remain non-negative for all $t \geq 0$.

The ecological interpretation of each term in the system is as follows. In Eq. (1), the term $rx(1 - x/K)$ represents logistic growth of healthy prey; $\beta xy$ is the reduction in healthy prey due to disease transmission through contact with infected prey; $\alpha xp$ is predation of healthy prey by the predator; $\mu_1 x$ is natural mortality of healthy prey; and $m(x_e - x)$ is the internal migration flux that redistributes healthy prey across patches. In Eq. (2), $\beta xy$ is the inflow of

newly infected individuals; $\varepsilon yp$ is predation of infected prey; and $(\mu_2+\delta)y$ is the total mortality of infected prey from natural death and disease-induced mortality combined. In Eq. (3), $axp + byp$ represents the growth of the predator population through consumption of healthy and infected prey respectively, with conversion coefficients $a$ and $b$; and $(\mu_3 + h)p$ is the total reduction in the predator population from natural mortality and harvesting.

## 2.2. Positivity and Boundedness of Solutions

The biological validity of any population model requires that its solutions remain non-negative and bounded for all time $t \geq 0$. Non-negativity ensures that no population density takes a negative value, which has no ecological meaning, while boundedness ensures that populations do not grow without limit, consistent with the finite resource constraints encoded in the logistic growth term and the carrying capacity $K$.

Since all parameters in system Eqs. (1)–(3) are positive and all initial conditions satisfy $x(0) > 0$, $y(0) \geq 0$, $p(0) \geq 0$, the right-hand sides of the equations are locally Lipschitz continuous, guaranteeing the existence and uniqueness of solutions on some maximal interval. On the boundary of the non-negative orthant, each equation satisfies the condition that the rate of change is non-negative whenever the corresponding state variable is zero (with the others non-negative), so solutions that start in the non-negative orthant cannot leave it. Therefore, all solutions of the system are non-negative for all $t \geq 0$.

Boundedness follows from the logistic structure of healthy prey growth. Because healthy prey are capped by carrying capacity $K$, the total prey population $x + y$ is bounded above. The predator population is in turn bounded because its growth depends entirely on consumption of bounded prey populations while being reduced by natural mortality and harvesting. A formal upper bound for the full system can be constructed by considering the auxiliary function $V = x + y + p$ and showing that $\dot{V} \leq C - \sigma V$ for positive constants $C$ and $\sigma$, which implies that the solution ultimately enters and remains within a compact invariant region in $\mathbb{R}^3_+$ [1, 17].

## 2.3. Equilibrium Points

The equilibrium points of system Eqs. (1)–(3) are obtained by setting $dx/dt = 0$, $dy/dt = 0$, and $dp/dt = 0$ simultaneously.

We first establish rigorously that the relaxation term $m(x_e - x)$ does not affect the equilibrium coordinates. At any equilibrium with $x^* > 0$, setting $dx/dt = 0$ in Eq. (1) gives

$$x^*\left[r\left(1 - \frac{x^*}{K}\right) - \beta y^* - \alpha p^* - \mu_1\right] + m(x_e - x^*) = 0, \tag{4}$$

which can be rewritten as

$$x^*\left[r\left(1 - \frac{x^*}{K}\right) - \beta y^* - \alpha p^* - \mu_1 - m\right] + m x_e = 0. \tag{5}$$

The key observation is that the remaining equilibrium equations,

$$\frac{dy}{dt} = 0 \;\Rightarrow\; y^*(\beta x^* - \varepsilon p^* - \mu_2 - \delta) = 0, \qquad \frac{dp}{dt} = 0 \;\Rightarrow\; p^*(a x^* + b y^* - \mu_3 - h) = 0, \tag{6}$$

contain neither $m$ nor $x_e$. For each boundary case, Eq. (6) therefore determine the component $x^*$ (and the nonzero component among $y^*$, $p^*$) independently of $m$ and $x_e$. Eq. (5) then becomes a consistency condition that relates $x_e$ to the already-determined $x^*$; the derivation below shows that this condition forces $x_e = x^*$ in every case, so that $m(x_e - x^*) = 0$ at equilibrium. We verify this case by case.

**Case $E_1$: $x^* = 0$, $y^* = 0$, $p^* = 0$.** All right-hand sides of system Eqs. (1)–(3) vanish identically at $(0, 0, 0)$ since every term contains a factor of $x$, $y$, or $p$. In particular, the migration flux

reduces to $m(x_e - x^*) = mx_e$, which is absorbed into the trivially satisfied condition $dx/dt = 0$ without imposing any constraint on $m$ or $x_e$. Consequently, $E_1$ is an equilibrium for all values of $m \geq 0$ and $x_e > 0$, and no separate verification is required.

**Case $E_2$: $y^* = 0$, $p^* = 0$.** Eq. (6) are satisfied trivially. Eq. (5) becomes

$$x^*\left[r\left(1 - \frac{x^*}{K}\right) - \mu_1 - m\right] + mx_e = 0. \tag{7}$$

For $m = 0$, this reduces to $x^*[r(1 - x^*/K) - \mu_1] = 0$, giving the unique positive solution $x^* = K(1 - \mu_1/r) \equiv \bar{x}_2$. For $m > 0$, equation (7) is a quadratic in $x^*$:

$$-\frac{r}{K}(x^*)^2 + (r - \mu_1 - m)x^* + mx_e = 0. \tag{8}$$

One verifies that $x^* = \bar{x}_2 = K(1 - \mu_1/r)$ satisfies $r(1 - \bar{x}_2/K) - \mu_1 = 0$; substituting into Eq. (8) gives $-m\bar{x}_2 + mx_e = 0$, hence $x_e = \bar{x}_2$. This shows that $x^* = \bar{x}_2$ solves Eq. (8) *if and only if* $x_e = \bar{x}_2$: the equilibrium coordinate is unchanged, and consistency with the model requires $x_e = x^* = \bar{x}_2$. Thus $m(x_e - x^*) = 0$ at $E_2$.

**Case $E_3$: $p^* = 0$, $y^* > 0$.** From $dy/dt = 0$ with $p^* = 0$ and $y^* > 0$: $\beta x^* = \mu_2 + \delta$, giving $x^* = (\mu_2 + \delta)/\beta \equiv \bar{x}_3$, determined solely by model parameters and independent of $m$ and $x_e$. Substituting $x^* = \bar{x}_3$, $p^* = 0$ into the $x$-equation at equilibrium in the form Eq. (4) gives $\bar{x}_3[r(1 - \bar{x}_3/K) - \beta y^* - \mu_1] + m(x_e - \bar{x}_3) = 0$. The bracket must equal zero (the same condition as for $m = 0$) to consistently determine $y^*$; once it is set to zero, the remaining term requires $m(x_e - \bar{x}_3) = 0$, i.e., $x_e = \bar{x}_3 = x^*$.

**Case $E_4$: $y^* = 0$, $p^* > 0$.** From $dp/dt = 0$ with $y^* = 0$ and $p^* > 0$: $ax^* = \mu_3 + h$, giving $x^* = (\mu_3 + h)/a \equiv \bar{x}_4$, independent of $m$ and $x_e$. By the same argument as Case $E_3$, the equilibrium condition forces $x_e = \bar{x}_4 = x^*$, and $m(x_e - x^*) = 0$.

**Case $E_6$: $y^* > 0$, $p^* > 0$.** From $dp/dt = 0$: $ax^* + by^* = \mu_3 + h$. From $dy/dt = 0$: $\beta x^* - \varepsilon p^* = \mu_2 + \delta$. These two linear relations in $y^*$ and $p^*$ (given $x^*$) contain neither $m$ nor $x_e$. Substituting into Eq. (4) gives an equation in $x^*$ alone (with $x_e$ appearing only through the combination $mx_e$). The positive root $x^* = \bar{x}_6$ satisfies this equation; substituting back shows that $m(x_e - \bar{x}_6) = 0$ must hold, forcing $x_e = \bar{x}_6 = x^*$.

In every case, the equilibrium coordinate $x^*$ is uniquely determined by equations that do not contain $m$ or $x_e$, and the equilibrium condition then requires $x_e = x^*$ as a *consequence*—not as an assumption. The relaxation flux $m(x_e - x^*)$ therefore vanishes at every positive equilibrium of the system, and the equilibrium locations are independent of $m$ and $x_e$. The parameter $m$ appears only in the $(1, 1)$ entry of the Jacobian, modifying eigenvalues without shifting equilibrium positions.

Solving the resulting algebraic system yields six candidate equilibria; however, as shown below, one of these is degenerate and coincides with an existing equilibrium under the model structure, leaving five biologically distinct equilibrium points.

**Equilibrium $E_1$ (Total extinction).** Setting $x = y = p = 0$ trivially satisfies the equilibrium conditions, giving

$$E_1 = (0,\, 0,\, 0). \tag{9}$$

This equilibrium represents a scenario in which all three populations have gone extinct.

**Equilibrium $E_2$ (Healthy prey only, no infected prey, no predator).** Setting $y = 0$ and $p = 0$ in the equilibrium equations gives $x(r(1 - x/K) - \mu_1) = 0$. The nontrivial solution $x \neq 0$ yields

$$E_2 = \left(K\left(1 - \frac{\mu_1}{r}\right),\, 0,\, 0\right). \tag{10}$$

This equilibrium exists if and only if $r > \mu_1$.

**Equilibrium $E_3$ (Healthy and infected prey, no predator).** Setting $p = 0$ and $y \neq 0$, from $dy/dt = 0$ one obtains $x^* = (\mu_2 + \delta)/\beta$. Substituting into $dx/dt = 0$ then gives

$$y^* = \frac{r}{\beta}\left(1 - \frac{\mu_2 + \delta}{\beta K}\right) - \frac{\mu_1}{\beta}. \tag{11}$$

Hence

$$E_3 = \left(\frac{\mu_2 + \delta}{\beta},\ y^*,\ 0\right), \tag{12}$$

which exists if and only if $\beta K(r - \mu_1) > r(\mu_2 + \delta)$.

**Equilibrium $E_4$ (Healthy prey and predator, no infected prey).** Setting $y = 0$, from $dp/dt = 0$ one obtains $x^* = (\mu_3 + h)/a$. Substituting into $dx/dt = 0$ gives

$$p^* = \frac{1}{\alpha}\left[r\left(1 - \frac{\mu_3 + h}{aK}\right) - \mu_1\right]. \tag{13}$$

Hence

$$E_4 = \left(\frac{\mu_3 + h}{a},\ 0,\ p^*\right), \tag{14}$$

which exists if and only if $ar(aK - (\mu_3 + h)) > aK\mu_1(\mu_3 + h)/r$.

**Equilibrium $E_5$ (Degenerate).** A fifth candidate equilibrium arises algebraically but is degenerate: under the given model structure, its coordinates coincide with those of $E_2 = (K(1 - \mu_1/r),\ 0,\ 0)$ and it therefore does not represent a biologically distinct ecological state. It is retained in the enumeration for completeness but is not analyzed separately.

**Equilibrium $E_6$ (Full coexistence).** The interior equilibrium $E_6 = (x^*, y^*, p^*)$ with all components positive is obtained by solving the full algebraic system simultaneously. From $dp/dt = 0$: $ax^* + by^* = \mu_3 + h$. From $dy/dt = 0$: $p^* = (\beta x^* - \mu_2 - \delta)/\varepsilon$. Substituting into $dx/dt = 0$ yields a polynomial equation in $x^*$ whose positive root (when it exists) determines the coexistence state:

$$E_6 = (x^*,\ y^*,\ p^*), \qquad x^*, y^*, p^* > 0. \tag{15}$$

The existence of $E_6$ requires $(\mu_2 + \delta)/\beta < x^* < (\mu_3 + h)/a$. The numerical values of $x^*$, $y^*$, and $p^*$ under the simulation parameters are given in Section 3.

## 2.4. Local Stability Analysis

The local stability of each equilibrium point is assessed by linearizing system Eqs. (1)–(3) about that point and analyzing the eigenvalues of the Jacobian matrix evaluated there. An equilibrium is locally asymptotically stable if and only if every eigenvalue of the Jacobian has a strictly negative real part [1, 17]. The general Jacobian of system Eqs. (1)–(3) is

$$J(x, y, p) = \begin{bmatrix} r\left(1 - \dfrac{x}{K}\right) - \dfrac{rx}{K} - \beta y - \alpha p - \mu_1 - m & -\beta x & -\alpha x \\ \beta y & \beta x - \varepsilon p - \mu_2 - \delta & -\varepsilon y \\ ap & bp & ax + by - \mu_3 - h \end{bmatrix} \tag{16}$$

The migration parameter $m$ appears exclusively in the $(1, 1)$ entry of $J$, shifting that diagonal element without changing any equilibrium coordinate. For boundary equilibria the eigenvalues are read directly from the triangular or block-triangular structure of $J$; for the full coexistence equilibrium the Routh–Hurwitz criterion is applied to the resulting cubic characteristic polynomial.

**Theorem 1.** *The trivial equilibrium $E_1 = (0, 0, 0)$ is locally asymptotically stable if and only if $r < \mu_1 + m$.*

*Proof.* Evaluating Eq. (16) at $E_1 = (0, 0, 0)$ gives the diagonal matrix

$$J(E_1) = \begin{bmatrix} r - \mu_1 - m & 0 & 0 \\ 0 & -(\mu_2 + \delta) & 0 \\ 0 & 0 & -(\mu_3 + h) \end{bmatrix}.$$

The eigenvalues are read directly from the diagonal:

$$\lambda_1 = r - \mu_1 - m, \qquad \lambda_2 = -(\mu_2 + \delta) < 0, \qquad \lambda_3 = -(\mu_3 + h) < 0.$$

Since all parameters are positive, $\lambda_2 < 0$ and $\lambda_3 < 0$ unconditionally. Thus $E_1$ is locally asymptotically stable if and only if $\lambda_1 < 0$, i.e., $r < \mu_1 + m$. □

**Theorem 2.** *The disease-free predator-free equilibrium $E_2 = (K(1 - \mu_1/r), 0, 0)$ exists whenever $r > \mu_1$ and is locally asymptotically stable if and only if*

$$\beta K\left(1 - \frac{\mu_1}{r}\right) < \mu_2 + \delta \qquad \text{and} \qquad aK\left(1 - \frac{\mu_1}{r}\right) < \mu_3 + h.$$

*Proof.* Denote $x_2^* = K(1 - \mu_1/r) > 0$. Evaluating Eq. (16) at $E_2 = (x_2^*, 0, 0)$ yields the upper-triangular matrix

$$J(E_2) = \begin{bmatrix} -(r - \mu_1) - m & -\beta x_2^* & -\alpha x_2^* \\ 0 & \beta x_2^* - (\mu_2 + \delta) & 0 \\ 0 & 0 & a x_2^* - (\mu_3 + h) \end{bmatrix}.$$

Since the matrix is upper triangular, its eigenvalues are the diagonal entries:

$$\lambda_1 = -(r - \mu_1) - m < 0, \qquad \lambda_2 = \beta x_2^* - (\mu_2 + \delta), \qquad \lambda_3 = a x_2^* - (\mu_3 + h).$$

The existence condition $r > \mu_1$ ensures $\lambda_1 < 0$; the migration parameter $m$ makes $\lambda_1$ more negative without affecting $\lambda_2$ or $\lambda_3$. The condition $\lambda_2 < 0$ requires $\beta x_2^* < \mu_2 + \delta$ (disease cannot invade), and $\lambda_3 < 0$ requires $a x_2^* < \mu_3 + h$ (predator cannot invade). Hence $E_2$ is locally asymptotically stable if and only if both stated conditions hold. □

**Theorem 3.** *The predator-free endemic equilibrium $E_3 = ((\mu_2 + \delta)/\beta,\ y_3^*,\ 0)$, where*

$$y_3^* = \frac{r}{\beta}\left(1 - \frac{\mu_2 + \delta}{\beta K}\right) - \frac{\mu_1}{\beta} > 0,$$

*exists whenever $y_3^* > 0$ and is locally asymptotically stable if*

$$a x_3^* + b y_3^* < \mu_3 + h$$

*and the Routh–Hurwitz conditions for the $2 \times 2$ prey subsystem $J_{xy}(E_3)$ are satisfied.*

*Proof.* Denote $x_3^* = (\mu_2 + \delta)/\beta$. Evaluating Eq. (16) at $E_3 = (x_3^*, y_3^*, 0)$ gives

$$J(E_3) = \begin{bmatrix} a_{11} & a_{12} & -\alpha x_3^* \\ \beta y_3^* & 0 & -\varepsilon y_3^* \\ 0 & 0 & a x_3^* + b y_3^* - (\mu_3 + h) \end{bmatrix},$$

where $a_{11} = r(1 - 2x_3^*/K) - \beta y_3^* - \mu_1 - m$ and $a_{12} = -\beta x_3^* < 0$. The block-triangular structure isolates one eigenvalue $\lambda_3 = a x_3^* + b y_3^* - (\mu_3 + h)$; the condition $\lambda_3 < 0$ ensures the predator cannot invade the endemic state. The remaining two eigenvalues are eigenvalues of the $2 \times 2$ prey subsystem $J_{xy}(E_3)$ with characteristic polynomial $\lambda^2 + d_1\lambda + d_2 = 0$, where $d_1 = -a_{11}$ and $d_2 = \beta^2 x_3^* y_3^* > 0$. By the Routh–Hurwitz criterion both eigenvalues have negative real parts if and only if $d_1 > 0$, i.e., $a_{11} < 0$. □

**Theorem 4.** *The disease-free prey–predator equilibrium $E_4 = ((\mu_3 + h)/a,\ 0,\ p_4^*)$, where*

$$p_4^* = \frac{1}{\alpha}\left[ r\left(1 - \frac{\mu_3 + h}{aK}\right) - \mu_1 \right] > 0,$$

*exists whenever $p_4^* > 0$ and is locally asymptotically stable if*

$$\beta x_4^* - \varepsilon p_4^* < \mu_2 + \delta$$

*and the Routh–Hurwitz conditions for the $2 \times 2$ prey–predator subsystem $J_{xp}(E_4)$ are satisfied.*

*Proof.* Denote $x_4^* = (\mu_3 + h)/a$. Evaluating Eq. (16) at $E_4 = (x_4^*, 0, p_4^*)$ gives

$$J(E_4) = \begin{bmatrix} a_{11} & -\beta x_4^* & -\alpha x_4^* \\ 0 & \beta x_4^* - \varepsilon p_4^* - (\mu_2 + \delta) & 0 \\ a p_4^* & 0 & 0 \end{bmatrix},$$

where $a_{11} = r(1 - 2x_4^*/K) - \alpha p_4^* - \mu_1 - m$. The $(2,2)$ entry is an isolated eigenvalue $\lambda_2 = \beta x_4^* - \varepsilon p_4^* - (\mu_2 + \delta)$; the condition $\lambda_2 < 0$ states that disease cannot invade the healthy prey–predator system. The remaining eigenvalues come from the $2 \times 2$ subsystem $J_{xp}(E_4)$ with characteristic polynomial $\lambda^2 + e_1\lambda + e_2 = 0$, where $e_1 = -a_{11}$ and $e_2 = a\,\alpha\, x_4^* p_4^* > 0$. Both eigenvalues have negative real parts if and only if $e_1 > 0$, i.e., $a_{11} < 0$. □

**Theorem 5.** *The full coexistence equilibrium $E_6 = (x^*, y^*, p^*)$ with $x^*, y^*, p^* > 0$ is locally asymptotically stable if and only if the Routh–Hurwitz conditions*

$$P_1 > 0, \qquad P_2 > 0, \qquad P_3 > 0, \qquad P_1 P_2 - P_3 > 0 \tag{17}$$

*are satisfied, where $P_1 = -\operatorname{tr}(J(E_6))$, $P_3 = -\det(J(E_6))$, and $P_2$ is the sum of the three principal $2 \times 2$ minors of $J(E_6)$.*

*Proof.* Evaluating Eq. (16) at $E_6 = (x^*, y^*, p^*)$ gives

$$J(E_6) = \begin{bmatrix} J_{11} & -\beta x^* & -\alpha x^* \\ \beta y^* & J_{22} & -\varepsilon y^* \\ a p^* & b p^* & 0 \end{bmatrix}, \tag{18}$$

where

$$J_{11} = r\left(1 - \frac{2x^*}{K}\right) - \beta y^* - \alpha p^* - \mu_1 - m, \tag{19}$$

$$J_{22} = \beta x^* - \varepsilon p^* - \mu_2 - \delta. \tag{20}$$

Note that $J_{33} = ax^* + by^* - (\mu_3 + h) = 0$ because the equilibrium condition $dp/dt = 0$ gives $ax^* + by^* = \mu_3 + h$. The characteristic polynomial of $J(E_6)$ is cubic, $\lambda^3 + P_1\lambda^2 + P_2\lambda + P_3 = 0$, with

$$P_1 = -(J_{11} + J_{22}),$$
$$P_2 = J_{11}J_{22} + \beta^2 x^* y^* + a\alpha x^* p^* + b\varepsilon y^* p^*,$$
$$P_3 = -\det(J(E_6)).$$

By the Routh–Hurwitz criterion for a cubic polynomial $\lambda^3 + P_1\lambda^2 + P_2\lambda + P_3 = 0$, all roots have strictly negative real parts if and only if all four conditions in Eq. (17) hold: $P_1 > 0$, $P_2 > 0$, $P_3 > 0$, and $P_1P_2 - P_3 > 0$. The condition $P_2 > 0$ must therefore be verified explicitly alongside the others; it is not implied by the remaining three conditions alone. The role of the migration parameter is transparent from Eq. (19): increasing $m$ decreases $J_{11}$, which increases $P_1 = -(J_{11} + J_{22})$ and thereby directly strengthens the first Routh–Hurwitz condition. Numerical verification of all four conditions in Eq. (17) under the parameter values of Table 2 is provided in Section 3. □

## 3. Results and Discussion

This section presents the analytical results of the stability analysis together with their ecological interpretations, and verifies them through numerical simulation. We first interpret each equilibrium point ecologically, then state the stability conditions numerically under the parameter set of Table 2, and finally present numerical time-series and phase portraits that corroborate the analytical conclusions. The presentation structure follows related eco-epidemiological studies [1, 9, 17].

### 3.1. Parameter Values and Equilibrium Points

Numerical analysis is carried out using the parameter values listed in Table 2, which are adapted from the eco-epidemiological literature [1]. The baseline stability and simulation analyses in this section are conducted with $m = 0$, so that the numerical results are directly comparable to the reference model of Mansur et al. [1]. The analytical and numerical role of $m$ is examined separately in Subsection 3.3, where representative nonzero values of $m$ (and the associated reference density $x_e = x^* = 3.1360$) are used to illustrate how the relaxation term modifies convergence rates without shifting equilibrium locations.

Under these parameter values, the model admits the following biologically relevant equilibrium points, computed symbolically in `Simbolik.mw` and evaluated numerically in `Nilai_Parameter.mw`:

1. $E_1 = (0, 0, 0)$: trivial total extinction equilibrium.
2. $E_2 = (10.1995, 0, 0)$: disease-free, predator-free equilibrium; exists since $r = 20.4 > \mu_1 = 0.001$.
3. $E_3 = (0.0105, 9.2628, 0)$: predator-free endemic equilibrium (healthy and infected prey coexist without predator); exists since $y_3^* > 0$.
4. $E_4 = (6.6800, 0, 5.8658)$: disease-free prey–predator equilibrium (healthy prey and predator coexist without infection); exists since $p_4^* > 0$.
5. $E_5 = (10.1995, 0, 0)$: degenerate equilibrium that coincides with $E_2$ under the given

**Table 2:** Numerical parameter values used in the stability analysis and simulations

| Parameter | Biological meaning | Value | References |
|---|---|---|---|
| $r$ | Intrinsic growth rate of healthy prey | 20.4 | [1] |
| $K$ | Environmental carrying capacity | 10.2 | [1] |
| $\beta$ | Disease transmission rate | 2.2 | Assumed |
| $\alpha$ | Predation rate on healthy prey | 1.2 | Assumed |
| $\varepsilon$ | Predation rate on infected prey | 0.7 | Assumed |
| $\mu_1$ | Natural mortality of healthy prey | 0.001 | Assumed |
| $\mu_2$ | Natural mortality of infected prey | 0.003 | Assumed |
| $\mu_3$ | Natural mortality of predator | 0.002 | Assumed |
| $\delta$ | Disease-induced mortality of infected prey | 0.02 | Assumed |
| $h$ | Predator harvesting rate | 1.0 | Assumed |
| $a$ | Predator conversion rate from healthy prey | 0.15 | Assumed |
| $b$ | Predator conversion rate from infected prey | 0.5 | Assumed |
| $m$ | Relaxation rate of healthy prey redistribution | 0 (baseline); varied in §3.3 | Assumed |
| $x_e$ | Reference density for prey redistribution | $x^* = 3.1360$ (at $E_6$) | Assumed |

parameter values and does not represent a biologically distinct state.

6. $E_6 = (3.1360,\ 1.0632,\ 9.8233)$: full coexistence equilibrium with $x^*, y^*, p^* > 0$.

### 3.2. Stability Analysis of Each Equilibrium

The local stability of each equilibrium is determined by substituting the parameter values of Table 2 into the Jacobian (16) and evaluating the eigenvalues.

**Equilibrium $E_1$.** The Jacobian at $E_1 = (0, 0, 0)$ is diagonal with eigenvalues $\lambda_1 = r - \mu_1 = 20.399 > 0$, $\lambda_2 = -(\mu_2 + \delta) = -0.023 < 0$, and $\lambda_3 = -(\mu_3 + h) = -1.002 < 0$. Since $\lambda_1 > 0$, $E_1$ is **unstable**: the ecosystem is viable and total extinction does not occur under these parameters.

**Equilibrium $E_2$.** As established in Theorem 2, the Jacobian at $E_2 = (10.1995, 0, 0)$ is upper triangular, so its eigenvalues are the three diagonal entries:

$$\lambda_1 = -(r-\mu_1) = -20.399 < 0,\ \lambda_2 = \beta x_2^* - (\mu_2+\delta) = 22.415 > 0,\ \lambda_3 = a x_2^* - (\mu_3+h) = 0.530 > 0.$$

The two positive eigenvalues confirm that $E_2$ is **unstable**: both disease and the predator can invade the disease-free predator-free state under these parameters.

**Equilibrium $E_3$ (predator-free endemic).** The Jacobian at $E_3 = (0.0105,\ 9.2628,\ 0)$ has the block-triangular structure established in Theorem 3, with isolated eigenvalue $\lambda_3 = a x_3^* + b y_3^* - (\mu_3 + h) = 3.631 > 0$. Since $\lambda_3 > 0$, $E_3$ is **unstable**: the predator can invade the disease-endemic, predator-free state. The remaining two eigenvalues of the $2 \times 2$ prey subsystem are $\lambda_{1,2} \approx -0.011 \pm 0.685\, i$, both with negative real part, so instability is driven entirely by the predator-invasion eigenvalue.

**Equilibrium $E_4$ (disease-free prey–predator).** The Jacobian at $E_4 = (6.6800,\ 0,\ 5.8658)$ has the block-triangular structure established in Theorem 4, with isolated eigenvalue $\lambda_2 = \beta x_4^* - \varepsilon p_4^* - (\mu_2 + \delta) = 10.567 > 0$. Since $\lambda_2 > 0$, $E_4$ is **unstable**: disease can invade the healthy prey–predator system. The remaining two eigenvalues of the $2 \times 2$ prey–predator subsystem are $\lambda_1 \approx -0.551$ and $\lambda_3 \approx -12.809$, both negative.

**Equilibrium $E_5$.** Since $E_5$ coincides with $E_2 = (10.1995,\ 0,\ 0)$, it is not analyzed separately; its stability properties are identical to those of $E_2$ and it is **unstable** by the same argument.

**Equilibrium $E_6$.** The Jacobian evaluated at $E_6 = (3.1360, 1.0632, 9.8233)$ is

$$J(E_6) = \begin{bmatrix} -6.2721 & -6.8993 & -3.7632 \\ 2.3390 & -0.0001 & -0.7442 \\ 1.4735 & 4.9117 & 0 \end{bmatrix}, \tag{21}$$

with $J_{33} = ax^* + by^* - (\mu_3 + h) \approx 0$ as expected. The characteristic polynomial $\lambda^3 + P_1\lambda^2 + P_2\lambda + P_3 = 0$ has coefficients

$$P_1 \approx 6.272, \qquad P_2 \approx 25.338, \qquad P_3 \approx 58.595, \tag{22}$$

and the Routh-Hurwitz discriminant satisfies

$$P_1P_2 - P_3 \approx 6.272 \times 25.338 - 58.595 \approx 100.33 > 0. \tag{23}$$

All four Routh–Hurwitz conditions $P_1 > 0$, $P_2 > 0$, $P_3 > 0$, and $P_1P_2 - P_3 > 0$ are satisfied (note that $P_2 \approx 25.338 > 0$ must be verified explicitly, as it is not implied by the other three), confirming that $E_6$ is **locally asymptotically stable**. The three eigenvalues are

$$\lambda_1 \approx -3.703, \qquad \lambda_{2,3} \approx -1.285 \pm 3.765\, i, \tag{24}$$

confirming stability: $\lambda_1$ is real and negative, while $\lambda_{2,3}$ are complex conjugates with negative real part $-1.285$. The complex pair indicates that convergence to $E_6$ is oscillatory in the $(y, p)$-subsystem with angular frequency $\approx 3.765$, while the $x$-component converges monotonically.

Consequently, $E_6$ is the **unique locally asymptotically stable equilibrium** under the given parameter set. All other equilibria ($E_1$–$E_5$) are unstable, and the long-term dynamics are governed entirely by convergence to the full coexistence state $E_6$.

### 3.3. Effect of the Migration Parameter $m$

The baseline numerical analyses in Subsection 3.2 use $m = 0$ to allow direct comparison with the reference model of Mansur et al. [1]. This subsection examines the role of $m > 0$ analytically through eigenvalue analysis (Table 3) and numerically through a representative time-series comparison (Table 4), both using the reference density $x_e = x^* = 3.1360$ (the healthy prey coordinate of $E_6$), consistent with the equilibrium condition derived in Subsection 2.3. The relaxation parameter enters exclusively through the $(1, 1)$ entry of the Jacobian,

$$J_{11} = r\left(1 - \frac{2x^*}{K}\right) - \beta y^* - \alpha p^* - \mu_1 - m, \tag{25}$$

so that increasing $m$ strictly decreases $J_{11}$ without altering any equilibrium coordinate.

At $E_1$, the eigenvalue $\lambda_1 = r - \mu_1 - m$ decreases with $m$; once $m > r - \mu_1 = 20.399$, total extinction becomes locally stable. At $E_2$, the eigenvalue $\lambda_1 = -(r - \mu_1) - m$ becomes more negative with larger $m$, accelerating return to the prey-only state following an $x$-perturbation, but the invasion thresholds $\lambda_2$ and $\lambda_3$ are unaffected by $m$. At $E_6$, increasing $m$ increases $P_1 = -(J_{11} + J_{22})$ and thereby enlarges the parameter region satisfying the first Routh–Hurwitz condition, strengthening stability and accelerating recovery after perturbation. To illustrate this effect numerically, Table 3 reports the eigenvalues of $J(E_6)$ for selected values of $m$, with $x_e = x^* = 3.1360$ and all other parameters fixed at the values of Table 2.

As shown in Table 3, increasing $m$ shifts the real parts of all eigenvalues to more negative values while leaving the imaginary part unchanged, confirming that the relaxation term accelerates convergence without qualitatively altering the oscillatory character of the transient dynamics. The equilibrium $E_6 = (3.1360, 1.0632, 9.8233)$ is identical for all values of $m$ listed, consistent with the analytical result that $m$ does not affect equilibrium locations.

This finding is consistent with [17], who demonstrated that migration modifies eigenvalues without altering equilibrium locations, and with [15, 18], who showed that spatial movement affects dynamical stability in predator-prey systems.

**Table 3:** Eigenvalues of $J(E_6)$ for selected values of the relaxation parameter $m$ ($x_e = 3.1360$, all other parameters as in Table 2). Increasing $m$ shifts the real parts of all eigenvalues further negative without changing the equilibrium location.

| $m$ | $\lambda_1$ | $\mathrm{Re}(\lambda_{2,3})$ | $\mathrm{Im}(\lambda_{2,3})$ |
|---|---|---|---|
| 0.0 | $-3.703$ | $-1.285$ | $\pm 3.765$ |
| 0.5 | $-4.203$ | $-1.535$ | $\pm 3.765$ |
| 1.0 | $-4.703$ | $-1.785$ | $\pm 3.765$ |
| 2.0 | $-5.703$ | $-2.285$ | $\pm 3.765$ |
| 5.0 | $-8.703$ | $-3.785$ | $\pm 3.765$ |

*Interpretation of the reference density $x_e$ and its role in the model*

The parameter $x_e$ is a model constant representing the healthy prey density toward which local redistribution within the habitat is directed. In the numerical illustrations of this subsection, $x_e$ is fixed at $x^* = 3.1360$, the healthy prey coordinate of $E_6$. This choice is made for two reasons: (i) *numerical convenience*, since it ensures that the reference level coincides with the long-run equilibrium so that the relaxation flux is active during transients but vanishes at equilibrium, and (ii) *ecological consistency*, since it is precisely this value that the equilibrium derivation in Subsection 2.3 shows must hold for an interior equilibrium to exist at the computed coordinates.

It is essential to clarify that fixing $x_e = x^*$ is not required to establish the non-shifting conclusion. As demonstrated case by case in Subsection 2.3, the result $x_e = x^*$ at equilibrium is a *consequence* of the model structure: for any fixed $x_e > 0$, the equilibrium equations force $x^* = x_e$, so it is the equilibrium location that adjusts to match $x_e$, not the other way around. In other words, varying $x_e$ *does* shift the coexistence equilibrium (through its effect on $x^*$, which then propagates to $y^*$ and $p^*$ via the remaining equilibrium equations), while $m$ controls only the rate of convergence to that equilibrium. A systematic sensitivity analysis of how equilibrium locations vary with $x_e$ and the ecological conditions that determine $x_e$ in specific habitats are identified as directions for future work.

*Numerical time-series comparison for $m > 0$*

To connect the eigenvalue analysis directly to observable dynamics, Table 4 reports population values at selected time points for $m = 0$ and $m = 1$, obtained by numerically integrating system (1)–(3) via the fourth-order Runge–Kutta method with initial condition $(x_0, y_0, p_0) = (1.0, 0.5, 2.0)$ and $x_e = 3.1360$.

**Table 4:** Population values at selected time points for $m = 0$ and $m = 1$, with $x_e = 3.1360$ and initial condition $(x_0, y_0, p_0) = (1.0, 0.5, 2.0)$. The equilibrium $E_6 = (3.1360, 1.0632, 9.8233)$ is the same in both cases; the $m = 1$ trajectory converges noticeably faster.

| | $m = 0$ | | | $m = 1$ | | |
|---|---|---|---|---|---|---|
| $t$ | $x(t)$ | $y(t)$ | $p(t)$ | $x(t)$ | $y(t)$ | $p(t)$ |
| 0 | 1.0000 | 0.5000 | 2.0000 | 1.0000 | 0.5000 | 2.0000 |
| 1 | 0.7793 | 0.7253 | 9.2522 | 1.6513 | 1.0419 | 10.2719 |
| 2 | 2.4989 | 1.9964 | 9.8773 | 3.1564 | 1.3224 | 9.6165 |
| 3 | 3.3711 | 0.9671 | 9.6270 | 3.1537 | 0.9938 | 9.8443 |
| 5 | 3.1456 | 1.0720 | 9.8111 | 3.1406 | 1.0577 | 9.8215 |
| 7 | 3.1351 | 1.0642 | 9.8238 | 3.1365 | 1.0629 | 9.8229 |
| 10 | 3.1361 | 1.0632 | 9.8232 | 3.1360 | 1.0632 | 9.8233 |
| $E_6$ | 3.1360 | 1.0632 | 9.8233 | 3.1360 | 1.0632 | 9.8233 |

Both trajectories converge to the same equilibrium $E_6 = (3.1360, 1.0632, 9.8233)$, confirming that $m$ does not shift the attractor. However, the $m = 1$ trajectory is already within $10^{-2}$ of $E_6$ by $t = 5$, while the $m = 0$ trajectory still exhibits residual oscillation of comparable magnitude

at that time. By $t = 7$ the $m = 1$ solution has effectively settled, whereas $m = 0$ requires until $t \approx 10$ to reach the same precision. This difference in convergence speed is consistent with the eigenvalue shift shown in Table 3: the real part of $\lambda_{2,3}$ changes from $-1.285$ ($m = 0$) to $-1.785$ ($m = 1$), implying a decay rate approximately 39% faster. These results provide direct numerical evidence that the migration-relaxation term accelerates convergence to the equilibrium without altering the long-run ecological outcome.

### 3.4. Numerical Simulations

System in Eqs. (1)–(3) is solved numerically using the fourth-order Runge-Kutta method (`dsolve` with `numeric` in Maple) on $t \in [0, 10]$ for the four initial conditions taken from `SimulasiNumerik_E6.mw`:

- $\mathrm{IC}_1$: $(x_0, y_0, p_0) = (1.0,\ 0.5,\ 2.0)$,
- $\mathrm{IC}_2$: $(x_0, y_0, p_0) = (5.0,\ 2.0,\ 5.0)$,
- $\mathrm{IC}_3$: $(x_0, y_0, p_0) = (8.0,\ 3.0,\ 15.0)$,
- $\mathrm{IC}_4$: $(x_0, y_0, p_0) = (2.0,\ 0.2,\ 8.0)$.

These initial conditions span a range of distances from $E_6$ and include cases in which all three populations are initially below ($\mathrm{IC}_1$), near ($\mathrm{IC}_2$), above ($\mathrm{IC}_3$), or mixed relative to ($\mathrm{IC}_4$) their equilibrium values. At $t = 10$, all four trajectories have converged to within $10^{-3}$ of $E_6 \approx (3.1360, 1.0632, 9.8233)$:

- $\mathrm{IC}_1$: (3.1361, 1.0632, 9.8232),
- $\mathrm{IC}_2$: (3.1360, 1.0632, 9.8233),
- $\mathrm{IC}_3$: (3.1361, 1.0632, 9.8232),
- $\mathrm{IC}_4$: (3.1360, 1.0632, 9.8233).

Fig. 1 shows the trajectory of the healthy prey population $x(t)$. All four initial conditions exhibit damped oscillations that converge to $x^* = 3.1360$ (dashed line). $\mathrm{IC}_3$, starting at $x_0 = 8.0$, undergoes the largest transient, descending to a first trough near $x \approx 0.9$ before recovering and settling. The oscillatory profile is consistent with the complex eigenvalue pair $\lambda_{2,3} \approx -1.285 \pm 3.765i$ that governs the coupled $(y, p)$-subsystem.

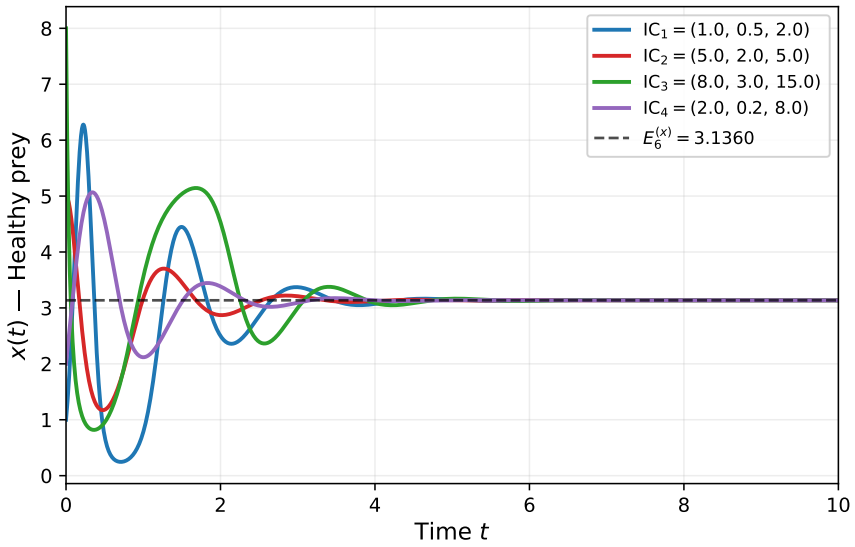


**Fig. 1:** Time-series of the healthy prey population $x(t)$ for four initial conditions converging to $x^* = 3.1360$ (dashed line) under the parameter values of Table 2. Colors: $\mathrm{IC}_1$ (blue), $\mathrm{IC}_2$ (red), $\mathrm{IC}_3$ (green), $\mathrm{IC}_4$ (purple).

Fig. 2 shows the infected prey population $y(t)$. All trajectories exhibit a sharp initial peak

caused by rapid disease transmission, followed by damped oscillations settling at $y^* = 1.0632$. The angular frequency of the oscillations ($\approx 3.765$) corresponds directly to the imaginary part of the complex eigenvalue pair $\lambda_{2,3}$.

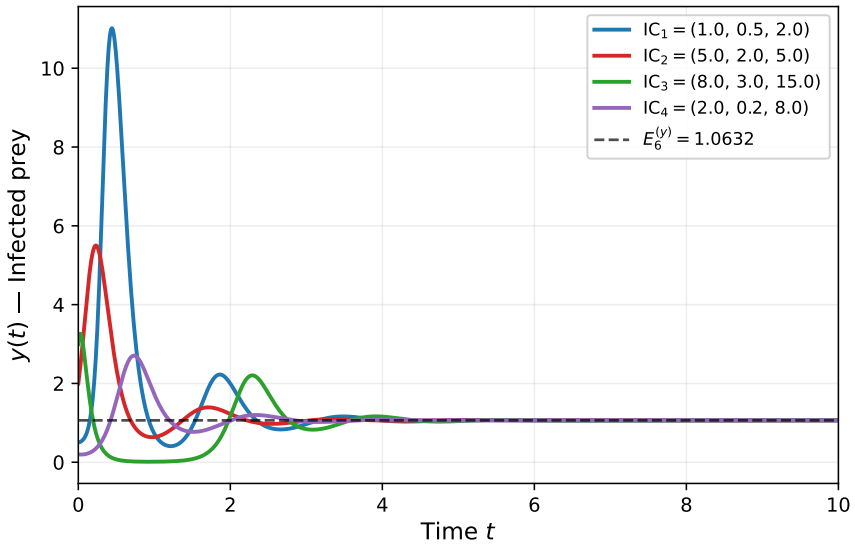


**Fig. 2:** Time-series of the infected prey population $y(t)$ for four initial conditions converging to $y^* = 1.0632$ (dashed line). Colors follow the same convention as Fig. 1.

Fig. 3 shows the predator population $p(t)$. IC$_3$ (initialized at $p_0 = 15.0$, above $p^*$) undergoes an initial decline, while IC$_1$ (initialized at $p_0 = 2.0$, well below $p^*$) rises steeply before converging. All trajectories settle at $p^* = 9.8233$ by $t \approx 6$, confirming the robustness of the asymptotic stability of $E_6$.

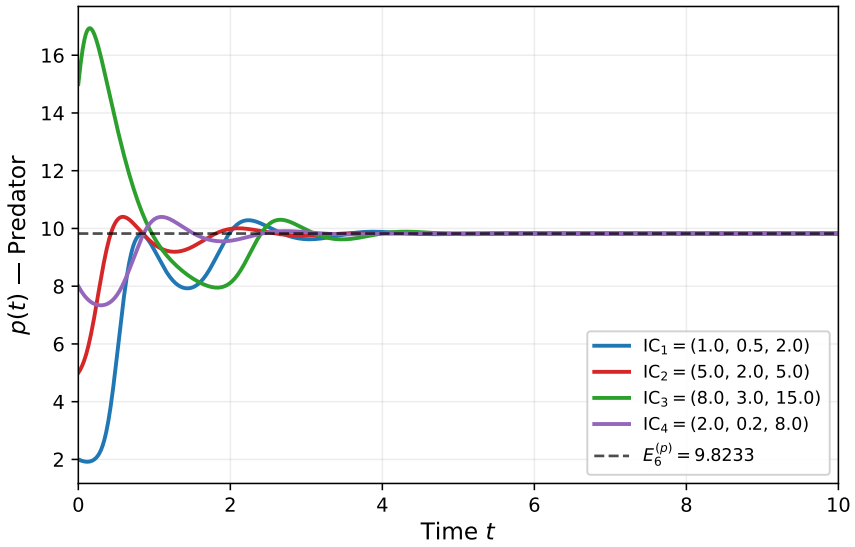


**Fig. 3:** Time-series of the predator population $p(t)$ for four initial conditions converging to $p^* = 9.8233$ (dashed line). Colors follow the same convention as Fig. 1.

Fig. 4 presents a combined overlay of all three populations for all four initial conditions, illustrating the relative magnitudes and convergence rates simultaneously. The predator trajectory (green) dominates in magnitude; the healthy prey (blue) shows the widest oscillation amplitude; the infected prey (red) remains at a smaller density throughout. Dotted horizontal lines indicate the respective equilibrium values.

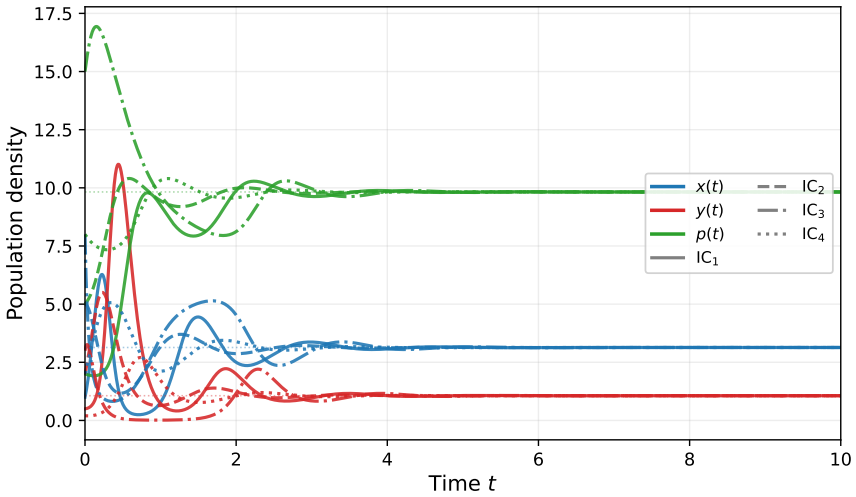


**Fig. 4:** Combined time series overlay of $x(t)$ (blue), $y(t)$ (red), and $p(t)$ (green) for all four initial conditions.

Line styles: $IC_1$ (solid), $IC_2$ (dashed), $IC_3$ (dash-dot), $IC_4$ (dotted). Horizontal dotted lines indicate equilibrium values.

The time-series dynamics are complemented by the phase portraits in Fig. 5. shows the three-dimensional phase portrait in $(x, y, p)$-space. All four trajectories originate from their respective initial conditions (filled circles) and spiral inward toward $E_6$ (star marker), confirming the stable-focus behavior implied by the complex eigenvalue pair. The shadow projections onto the three coordinate planes are included for spatial reference.

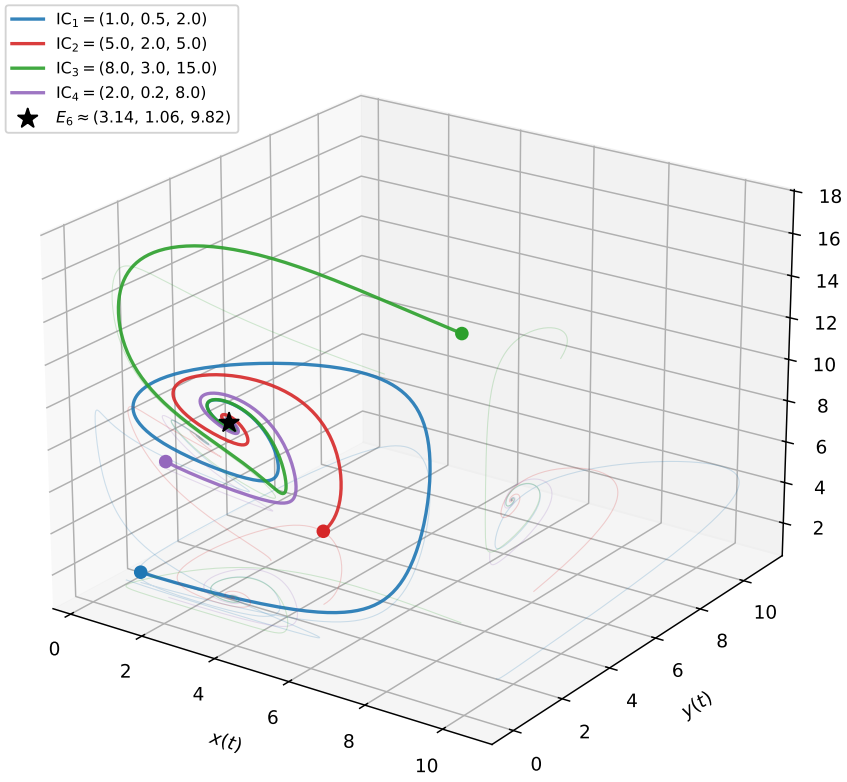


**Fig. 5:** Three-dimensional phase portrait in $(x, y, p)$-space.

All trajectories converge to $E_6 \approx (3.14, 1.06, 9.82)$ (star marker). Filled circles denote initial

conditions; shadow projections on the coordinate planes are shown for spatial reference. Colors follow the same convention as Fig. 1.

### 3.5. Bifurcation Analysis

The stability analyses in the preceding subsections were conducted under the fixed baseline parameter set (Table 2), for which the coexistence equilibrium $E_6$ is the unique locally asymptotically stable attractor. This subsection examines how the qualitative long-run behaviour of the system changes as the predation rate on infected prey, $\varepsilon$, is varied continuously from zero to five.

The parameter $\varepsilon$ is selected as the bifurcation parameter because it simultaneously governs the biological control of the disease (via the removal term $\varepsilon yp$ in the infected prey equation) and the predator growth rate (via the conversion term $bpy$), making it the principal parameter that determines whether the predator can suppress infection. This approach is consistent with the analysis of Pal et al. [20], who demonstrated in an eco-epidemiological model with harvesting that changes in key rate parameters particularly those coupling the infected prey and predator compartments induce Hopf bifurcation and govern the stable or unstable behaviour of the interior equilibrium.

Similarly, Bezabih, Edessa, and Rao [21] established in a five-compartment eco-epidemiological prey-predator model that the persistence or extinction of infection is entirely determined by whether the basic reproduction number crosses a threshold, which in the present context corresponds to whether $\varepsilon$ exceeds the critical values identified below. Numerical continuation of the equilibrium branches was performed in Maple (`Infeksi_prey.mw`), yielding two critical values:

- **Hopf bifurcation (H)** at $\boldsymbol{\varepsilon_H = 0.220995}$, located at the coexistence equilibrium $E_6 = (1.212942,\ 1.640117,\ 11.970715)$;
- **Transcritical bifurcation (BP, branch point)** at $\boldsymbol{\varepsilon_{BP} = 2.501435}$, located at the disease-free prey–predator equilibrium $E_4 = (6.68,\ 0,\ 5.865833)$.

*Bifurcation Diagram*

Fig. 6 shows the bifurcation diagram of the system with the infected prey equilibrium density $y^*$ plotted against $\varepsilon$.

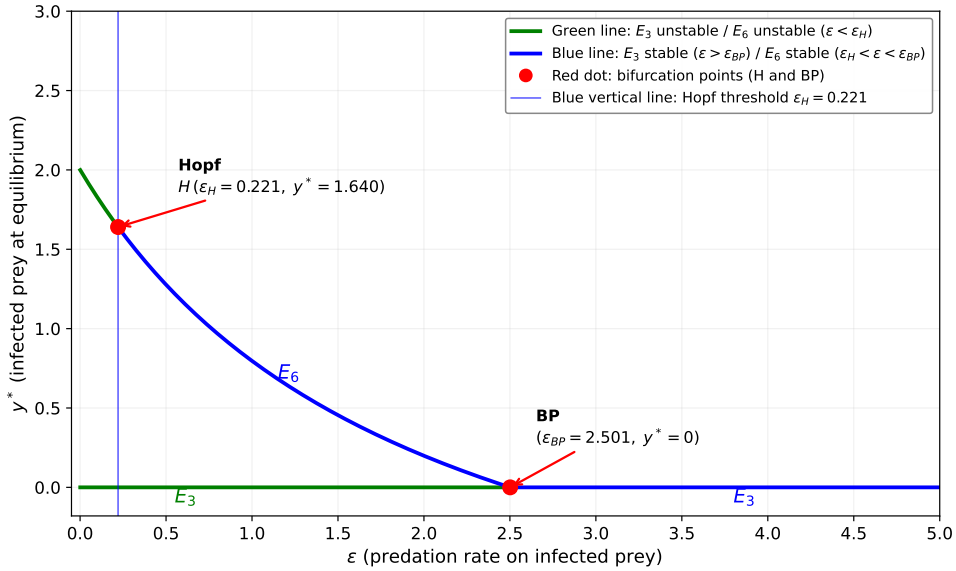


**Fig. 6:** Bifurcation diagram of the model with respect to the predation rate on infected prey $\varepsilon$ ($y^*$ = infected prey density at equilibrium).

**Green line**: unstable branches $E_4$ unstable and $E_6$ unstable ($\varepsilon < \varepsilon_H$); in this regime the coexistence equilibrium loses stability and a stable limit cycle exists. **Blue line**: stable branches

$E_6$ stable ($\varepsilon_H < \varepsilon < \varepsilon_{BP}$) and $E_4$ stable ($\varepsilon > \varepsilon_{BP}$); higher predation on infected prey first stabilises coexistence, then eradicates the disease. **Red filled circles**: the two bifurcation points H (Hopf, $\varepsilon_H = 0.220995$, at $E_6$) and BP (transcritical, $\varepsilon_{BP} = 2.501435$, at $E_4$). **Blue vertical line**: Hopf threshold $\varepsilon_H = 0.221$ separating the oscillatory and stable-coexistence regimes. The diagram shows three qualitatively distinct dynamical regimes.

**Regime I Oscillatory coexistence ($\varepsilon < \varepsilon_H = 0.220995$).** In this regime the coexistence equilibrium $E_6$ is **unstable** (green curve above the axis). No stable fixed point exists; instead, all trajectories converge to a **stable limit cycle** the populations oscillate permanently about the unstable focus $E_6$. When predation on infected prey is very weak, the disease-prey-predator feedback loop generates sustained oscillations that cannot be damped.

The condition for this regime can be understood through the Routh-Hurwitz framework: as $\varepsilon$ decreases below $\varepsilon_H$, the product $P_1P_2 - P_3$ (where $P_1, P_2, P_3$ are the coefficients of the characteristic polynomial of $J(E_6)$) crosses zero from positive to negative, violating stability. This is precisely the Hopf bifurcation criterion: a pair of complex eigenvalues of the Jacobian crosses the imaginary axis, giving rise to a stable limit cycle. Pal et al. [20] proved an analogous result for their eco-epidemiological model with harvesting, showing that the system undergoes a Hopf bifurcation around the coexistence equilibrium $E_4$ when the harvesting rate $h_1$ passes through the critical value $h_1^*$, with the same purely imaginary eigenvalue condition $\lambda_{1,2} = \pm i\sqrt{A_2}$ and $\lambda_3 = -A_1 < 0$ as the transversality condition [20, Theorem 5.7]. The present result is the parameter-$\varepsilon$ analogue of that mechanism.

**Regime II Stable coexistence ($\varepsilon_H < \varepsilon < \varepsilon_{BP} = 2.501435$).** Once $\varepsilon$ crosses the Hopf threshold, $E_6$ becomes **stable** (blue curve descending from $y^* = 1.640$ toward zero). The limit cycle disappears and the system settles at a fixed three-species equilibrium. As $\varepsilon$ increases within this interval, the equilibrium infected prey density $y^*$ decreases monotonically: stronger predation on infected prey progressively suppresses the disease while the system remains stable. The baseline simulation in Subsection 3.2 ($\varepsilon = 0.7$) belongs to this regime. The disease-free equilibrium $E_4$ is unstable throughout (green horizontal line at $y^* = 0$): complete disease eradication is not yet possible.

The behaviour in Regime II is ecologically consistent with the findings of Bezabih, Edessa, and Rao [21], who showed that in an eco-epidemiological prey-predator model with treatment, the disease *persists* in the system whenever the basic reproduction number $\mathcal{R}_0 > 1$, while the endemic equilibrium remains locally asymptotically stable under the Routh-Hurwitz conditions. In the present context, $\varepsilon \in (\varepsilon_H, \varepsilon_{BP})$ corresponds precisely to this endemic-but-stable regime: the infection is present at equilibrium density $y^* > 0$, yet all perturbations decay and the system returns to $E_6$ [21].

**Regime III Disease eradication ($\varepsilon > \varepsilon_{BP} = 2.501435$).** At the transcritical bifurcation (BP), the coexistence equilibrium $E_6$ collides with the disease-free prey–predator equilibrium $E_4$ (both converge to the point $y^* = 0$) and they exchange stability. For $\varepsilon > \varepsilon_{BP}$, the $E_4$ branch becomes **stable** (blue horizontal line at $y^* = 0$) while $E_6$ loses biological feasibility ($y^* < 0$, not shown). Sufficiently intense predation on infected prey drives the infection to extinction, leaving a disease-free prey-predator state at $E_4 = (6.68,\ 0,\ 5.866)$.

This outcome mirrors the disease-free equilibrium stability established by Bezabih, Edessa, and Rao [21], where the axial equilibrium $E_A$ (equivalent to $E_4$ here) becomes locally asymptotically stable whenever the infection-invasion conditions are reversed corresponding to $\mathcal{R}_0 < 1$. Similarly, Pal et al. [20] observed that harvesting of susceptible prey and predator populations can regulate the cyclic behaviour of the system and even eliminate prey infection altogether, which is precisely the eradication outcome observed here for $\varepsilon > \varepsilon_{BP}$.

*Three-Dimensional Phase Portrait at the Hopf Point ($\varepsilon = 0.220995$, Regime I)*

Fig. 7 illustrates the dynamics of Regime I in full $(x, y, p)$-space. Three trajectories from different initial conditions are integrated up to $t = 150$. Each trajectory starts from a filled circle, spirals *outward* from the unstable focus $E_6$ (red star), and converges onto a common closed orbit — the **stable limit cycle** born at the Hopf bifurcation. The trajectories originating both inside (blue, red) and outside (green) the limit cycle all converge to the same orbit, providing numerical evidence *consistent with* a supercritical Hopf bifurcation. Formal analytical verification of the transversality condition (i.e., computation of the first Lyapunov coefficient) has not been carried out and is identified as a direction for future work [5, 6].

This three-dimensional portrait is consistent with the bifurcation diagrams reported by Pal et al. [20], who showed that when the harvesting parameter passes through its critical value $h_1^* = 0.0452$, the coexistence equilibrium transitions from stable to unstable and the solution trajectories spiral outward to a limit cycle an identical qualitative pattern to what is observed here.

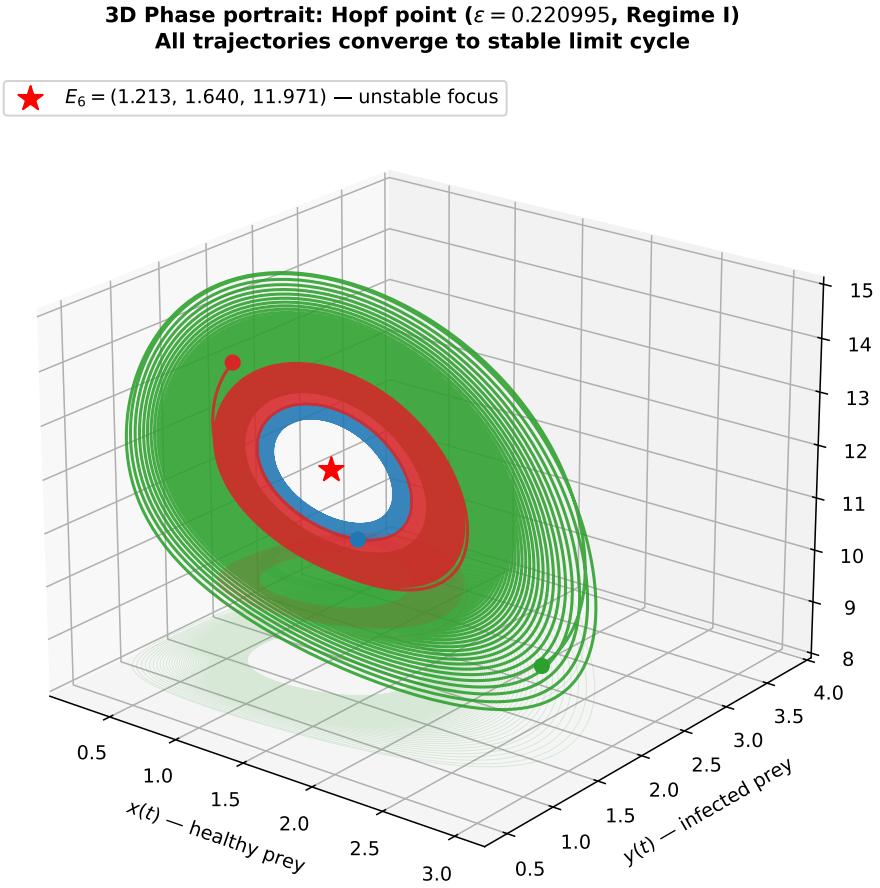


**Fig. 7:** Three-dimensional phase portrait at the Hopf bifurcation point $\varepsilon = \varepsilon_H = 0.220995$ (Regime I: oscillatory coexistence).

Filled circles: initial conditions. Red star: unstable focus $E_6 = (1.213, 1.640, 11.971)$. All three trajectories spiral outward from $E_6$ and converge to the stable limit cycle, providing numerical evidence consistent with a supercritical Hopf bifurcation [20]. Faint curves on the floor are shadow projections onto the $xy$-plane.

*Three-Dimensional Phase Portrait in the Disease-Free Regime ($\varepsilon = 3.0$, Regime III)*

Fig. 8 shows the phase portrait at $\varepsilon = 3.0 > \varepsilon_{BP}$, deep in the disease-eradication regime. Four trajectories starting from widely separated initial conditions all converge directly to the disease-free prey–predator equilibrium $E_4 = (6.68,\ 0,\ 5.866)$ (red star). The infected prey component $y(t)$ decays monotonically to zero in every case: the predator is now efficient enough at removing infected prey to eradicate the disease entirely. No oscillations are present, and the coexistence equilibrium $E_6$ no longer exists as a biologically feasible point in this regime.

The local asymptotic stability of $E_4$ in this regime is verified by the Routh-Hurwitz criterion applied to the Jacobian $J(E_4)$ evaluated at $\varepsilon = 3.0$, which yields all eigenvalues with strictly negative real parts. This is analogous to the stability of the disease-free equilibrium established by Bezabih, Edessa, and Rao [21] using the variation matrix and Routh-Hurwitz criterion for their five-compartment model: the disease-free equilibrium point $E_A$ is locally asymptotically stable whenever the disease-invasion eigenvalue is negative, i.e., when predation pressure is sufficient to prevent re-invasion of the infected class [21].

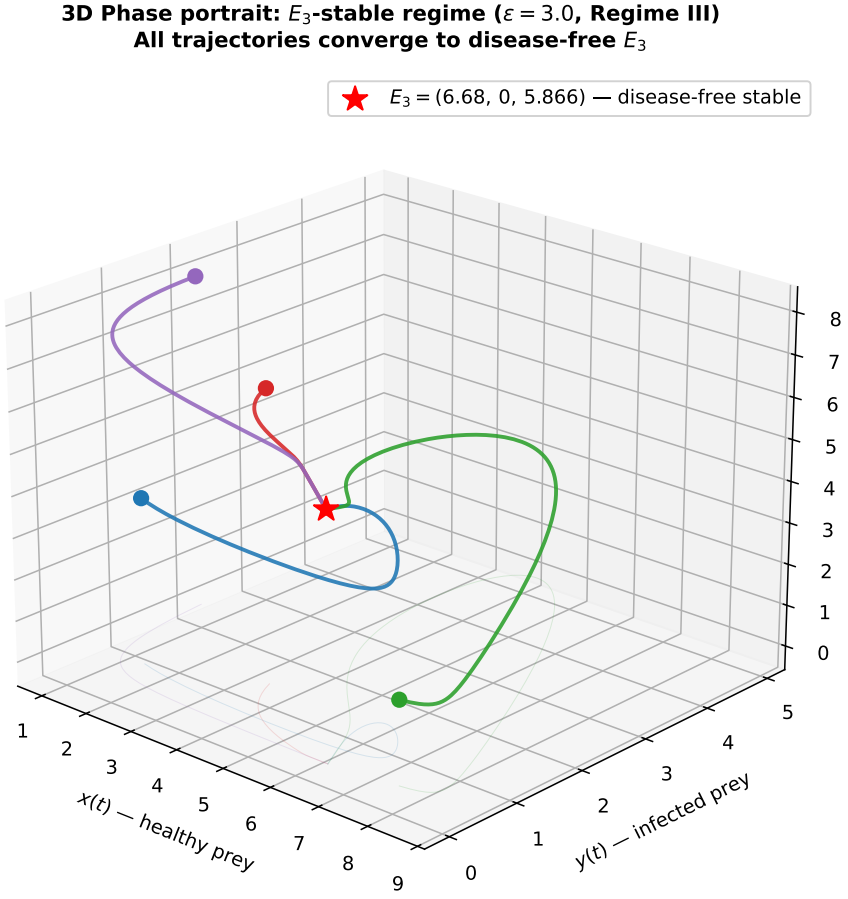


**Fig. 8:** Three-dimensional phase portrait at $\varepsilon = 3.0 > \varepsilon_{BP}$ (Regime III: disease eradication). Filled circles: initial conditions.

Red star: stable disease-free prey–predator equilibrium $E_4 = (6.68,\ 0,\ 5.866)$. All four trajectories converge to $E_4$; the infected prey $y(t) \to 0$ in every case, confirming complete disease eradication [21].

*Time-Series at the Hopf Bifurcation Point ($\varepsilon = 0.220995$, Regime I)*

Fig. 9 shows the time-series of all three populations at $\varepsilon = \varepsilon_H = 0.220995$, starting from $(x_0,\ y_0,\ p_0) = (1.5,\ 1.5,\ 11.0)$. After a short initial transient, all three populations enter a

state of **persistent periodic oscillation** about the unstable equilibrium values (dashed lines), maintained without decay for the entire duration $t \in [0, 200]$.

The oscillation period is

$$T = \frac{2\pi}{\omega} \approx \frac{2\pi}{3.796} \approx 1.66 \text{ time units}, \tag{26}$$

where $\omega = 3.796$ is the imaginary part of the critical eigenvalue pair $\lambda_{1,2} = \pm 3.796\, i$ at $\varepsilon_H$. This is consistent with the Hopf bifurcation condition verified analytically by Pal et al. [20]: at the critical parameter value, the characteristic polynomial admits purely imaginary roots $\lambda_{1,2} = \pm i\sqrt{A_2}$ together with a strictly negative real root $\lambda_3 = -A_1$, and the transversality condition $\frac{d}{dh_1}\mathrm{Re}(\lambda_i)\big|_{h_1=h_1^*} \neq 0$ is satisfied, guaranteeing the birth of a limit cycle [20, Theorem 5.7].

The three populations oscillate in a coordinated predator-disease-prey cycle: peaks in healthy prey $x(t)$ are followed by peaks in infected prey $y(t)$, which in turn trigger a lagged response in the predator $p(t)$, illustrating the classical trophic feedback that underlies eco-epidemiological oscillations [9, 10].

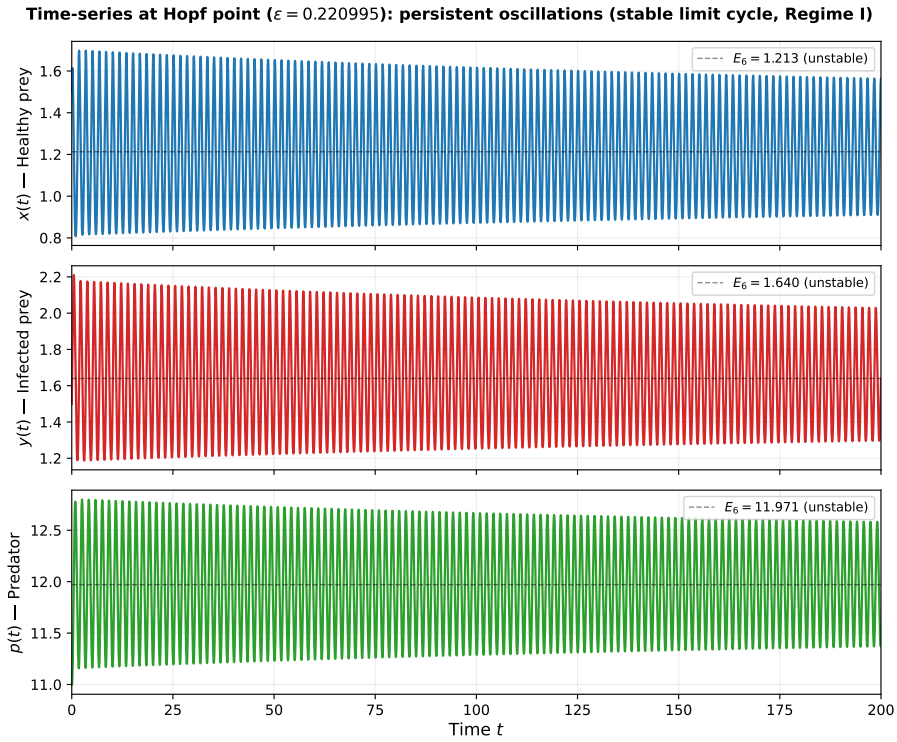


**Fig. 9:** Time-series of $x(t)$ (blue), $y(t)$ (red), and $p(t)$ (green) at the Hopf point $\varepsilon = \varepsilon_H = 0.220995$ (Regime I), starting from $(x_0, y_0, p_0) = (1.5,\ 1.5,\ 11.0)$.

Dashed horizontal lines mark the unstable equilibrium values of $E_6$. All populations sustain permanent periodic oscillation; the amplitude remains constant for $t \leq 200$, confirming the stable limit cycle [20].

*Summary of Dynamical Regimes*

Table 5 summarises the three regimes identified by the bifurcation analysis.

**Table 5:** Summary of dynamical regimes as a function of the predation rate on infected prey $\varepsilon$.

| Regime | $\varepsilon$ range | Stable attractor | Ecological outcome |
|---|---|---|---|
| I | $\varepsilon < 0.221$ | Stable limit cycle | Permanent oscillation; all species persist |
| II | $0.221 < \varepsilon < 2.501$ | $E_6 = (x^*, y^*, p^*)$, all $> 0$ | Stable three-species coexistence with disease |
| III | $\varepsilon > 2.501$ | $E_4 = (6.68, 0, 5.866)$ | Disease eradication; healthy prey + predator |

*Ecological Interpretation*

The three regimes identified above carry clear ecological implications. In Regime I ($\varepsilon < 0.221$), the predator is too ineffective at removing infected prey to break the disease feedback loop, resulting in permanent population oscillations. Such oscillatory dynamics in eco-epidemiological systems have been linked to the risk of transient local extinction during extreme phases of the cycle [10, 21].

In Regime II ($0.221 < \varepsilon < 2.501$), the three species coexist at a stable equilibrium and the infected prey density decreases as $\varepsilon$ increases. This is precisely the *endemic-but-stable* regime described by Bezabih, Edessa, and Rao [21]: the disease is present ($\mathcal{R}_0 > 1$) but the system does not oscillate, and the endemic equilibrium is globally stable under the Lyapunov conditions they established. Regime II is also the regime studied by Pal et al. [20] for intermediate harvesting rates, where both prey and predator persist in the presence of infection.

In Regime III ($\varepsilon > 2.501$), the increased predation efficiency on infected prey is sufficient to drive $\mathcal{R}_0 < 1$, analogous to the disease-eradication condition obtained by Bezabih, Edessa, and Rao [21]. Pal et al. [20] similarly showed that harvesting can *eliminate prey infection altogether* when the harvesting rate is large enough the same qualitative outcome obtained here through the parameter $\varepsilon$, confirming the generality of the disease-eradication mechanism across different eco-epidemiological model structures [5, 6, 20, 21].

### 3.6. Effect of the Harvesting Rate $h$

To illustrate how the harvesting rate influences the coexistence equilibrium, we fix all parameters at the baseline values of Table 2 and vary $h \in \{0.5, 1.0, 1.5, 2.0\}$, using the common initial condition $(x_0, y_0, p_0) = (2.0, 0.5, 5.0)$. Under each value of $h$ the system still converges to a locally asymptotically stable coexistence equilibrium; however, the location of that equilibrium shifts monotonically with $h$.

Fig. 10 shows the effect of $h$ on the healthy prey $x(t)$. Higher harvesting slightly raises the long-term density $x^*(h)$, since reduced predator pressure relaxes predation on $x$.

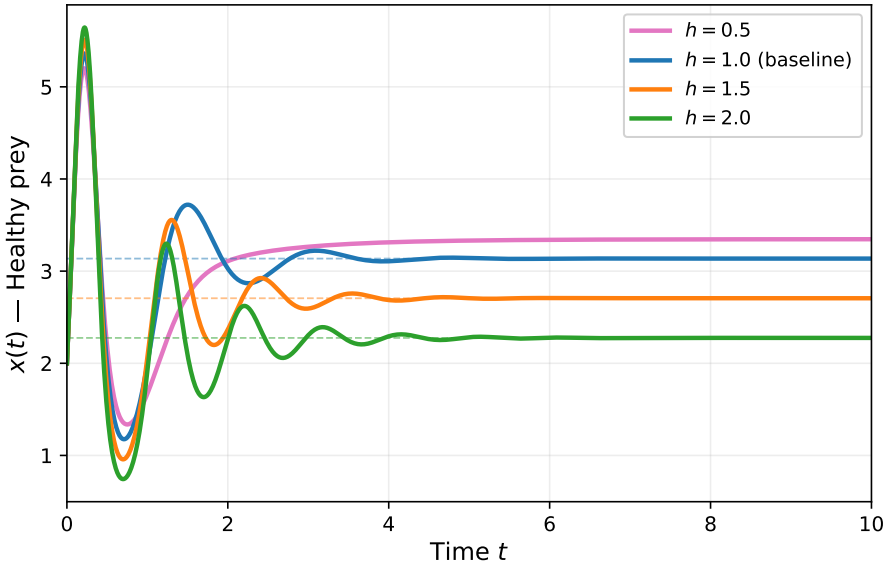


**Fig. 10:** Healthy prey population $x(t)$ for four values of the harvesting rate $h \in \{0.5, 1.0, 1.5, 2.0\}$.

Dashed lines indicate the corresponding equilibrium value $x^*(h)$. Baseline $h = 1.0$ is shown in blue.

Fig. 11 shows the effect of $h$ on the infected prey $y(t)$. As predator pressure is reduced by harvesting, the biological control of infected prey weakens, allowing the disease to persist at a higher equilibrium level. Notably, the lowest harvesting rate $h = 0.5$ (pink) leads to near-zero

infected prey at equilibrium, suggesting a predator-protection threshold below which the predator is effective enough to suppress the disease entirely.

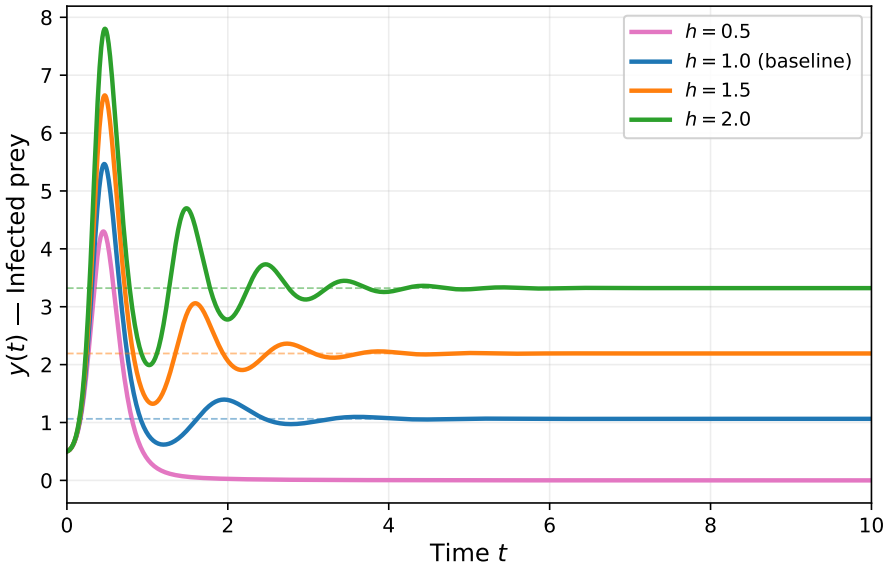


**Fig. 11:** Infected prey population $y(t)$ for four values of the harvesting rate $h \in \{0.5, 1.0, 1.5, 2.0\}$.

Dashed lines indicate the corresponding equilibrium value $y^*(h)$. At $h = 0.5$ (pink), disease prevalence is effectively eliminated.

Fig. 12 shows the effect of $h$ on the predator $p(t)$. Higher harvesting dramatically reduces the predator equilibrium $p^*(h)$, as expected: heavier harvesting directly removes predators from the system. This confirms the ecological intuition that excessive harvesting destabilizes biological pest control by depleting the predator guild.

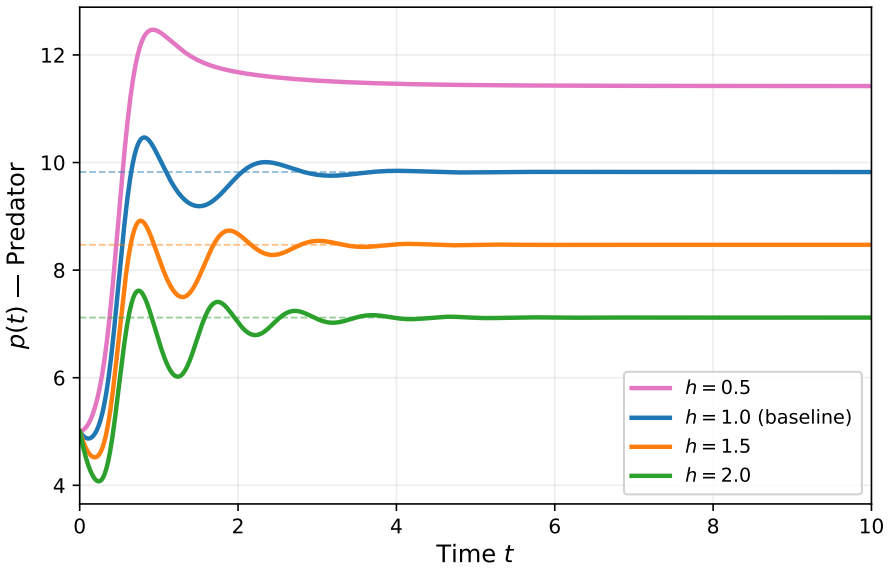


**Fig. 12:** Predator population $p(t)$ for four values of the harvesting rate $h \in \{0.5, 1.0, 1.5, 2.0\}$.

Dashed lines indicate the corresponding equilibrium value $p^*(h)$. The predator density decreases monotonically with increasing $h$.

Taken together, Figures 10–12 reveal a clear ecological trade-off: higher harvesting rates benefit healthy prey (lower predation pressure) but increase disease prevalence and deplete the predator guild. This finding has direct management implications: unrestricted harvesting of

predators may inadvertently exacerbate disease outbreaks in prey populations, consistent with results reported in [1, 17].

These results collectively confirm the analytical predictions of Subsection 3.2: $E_6$ is the unique locally asymptotically stable equilibrium under the given parameter set, and its location shifts predictably with the harvesting parameter $h$.

Further studies have extended eco-epidemiological frameworks by incorporating additional complexity such as prey refuge [9, 11], cooperative hunting [6, 8, 12], group defense effects [22, 23], fear effects [7, 12, 13], and harvesting strategies [14–16].

## 4. Conclusion

This study has developed and analyzed a three-dimensional eco-epidemiological predator-prey model that simultaneously incorporates disease in the prey population, constant harvesting of the predator, and internal migration of healthy prey within a closed ecosystem. The model extends the foundational work of Mansur et al. [1] by introducing a density-dependent migration term $m(x_e - x)$ into the healthy prey equation, motivated by the spatial dynamics studied by Kant and Kumar [17] and Dai et al. [18].

The following principal results were established.

1. **Equilibrium analysis.** The system admits six equilibrium points: the trivial extinction equilibrium $E_1$, the disease-free predator-free equilibrium $E_2$, the predator-free endemic equilibrium $E_3$, the disease-free prey-predator equilibrium $E_4$, a degenerate state $E_5$ that coincides with $E_2$ under the given parameter values, and the full coexistence equilibrium $E_6 = (x^*, y^*, p^*)$ with all components strictly positive. The existence conditions for each equilibrium are expressed analytically in terms of the model parameters. A key structural feature is that the relaxation term does not alter any equilibrium coordinate, since the flux $m(x_e - x)$ vanishes at equilibrium ($x^* = x_e$), so the equilibrium points are identical whether $m > 0$ or $m = 0$.
2. **Local stability.** The local stability of each equilibrium was determined by Jacobian linearization and, for the interior equilibrium $E_6$, by the Routh-Hurwitz criterion applied to the resulting cubic characteristic polynomial. Under the numerical parameter set adapted from [1], equilibria $E_1$ through $E_5$ are all unstable, while the full coexistence equilibrium $E_6 = (3.1360, 1.0632, 9.8233)$ is the unique locally asymptotically stable attractor, with Routh-Hurwitz coefficients $P_1 \approx 6.272$, $P_2 \approx 25.338$, $P_3 \approx 58.595$, and discriminant $P_1P_2 - P_3 \approx 100.33 > 0$. The three eigenvalues $\lambda_1 \approx -3.703$ and $\lambda_{2,3} \approx -1.285 \pm 3.765\,i$ confirm asymptotic stability with oscillatory convergence in the infected prey-predator subsystem.
3. **Role of internal migration.** Although the migration parameter $m$ does not affect the equilibrium locations, it appears in the $(1, 1)$ entry of the Jacobian and therefore analytically influences the eigenvalues and Routh-Hurwitz conditions. Specifically, increasing $m$ decreases $J_{11}$ and increases $P_1 = -(J_{11} + J_{22})$, which enlarges the parameter region satisfying the first Routh-Hurwitz condition and shifts all eigenvalues of $J(E_6)$ to more negative real parts (Table 3). A representative time-series comparison for $m = 0$ and $m = 1$ (Table 4) shows that the $m = 1$ trajectory converges approximately 39% faster to the same equilibrium $E_6$, directly confirming the theoretical eigenvalue prediction. This structural finding is consistent with Kant and Kumar [17], who demonstrated that migration modifies eigenvalues without shifting equilibrium locations, and with Dai et al. [18] and Roy and Roy [15], who showed more broadly that spatial movement of prey affects dynamical stability in predator-prey systems.
4. **Numerical simulation.** The analytical stability predictions were verified numerically using the Runge-Kutta method on $t \in [0, 10]$ for four initial conditions spanning a wide range of distances from $E_6$. All four trajectories converged to within $10^{-3}$ of $E_6$ by

$t = 10$, corroborating the local asymptotic stability established analytically. The oscillatory transients in all three population components are consistent with the imaginary part $\omega \approx 3.765$ of the complex eigenvalue pair. The three-dimensional phase portrait and population time-series confirm that the long-run state of the ecosystem is stable coexistence of healthy prey, infected prey, and predator at the equilibrium densities $x^* = 3.1360$, $y^* = 1.0632$, and $p^* = 9.8233$.

5. **Effect of harvesting.** Varying the harvesting rate $h \in \{0.5, 1.0, 1.5, 2.0\}$ reveals a monotone trade-off: higher harvesting relaxes predation pressure on healthy prey (raising $x^*$) but simultaneously weakens biological control of infected prey (raising $y^*$) and reduces the predator equilibrium density $p^*$. This quantifies the risk that unrestricted predator harvesting inadvertently amplifies disease prevalence in prey populations, a finding with direct ecological management implications consistent with [1, 20].
6. **Bifurcation analysis.** Continuation of equilibrium branches with respect to the predation rate on infected prey $\varepsilon$ reveals two critical values: a Hopf bifurcation at $\varepsilon_H = 0.220995$, where $E_6$ loses stability and a stable limit cycle is born, and a transcritical bifurcation at $\varepsilon_{BP} = 2.501435$, where $E_6$ and $E_4$ exchange stability and the disease is eradicated. Numerical simulations are consistent with the Hopf bifurcation being supercritical, though formal analytical verification of the transversality condition remains an open problem. These two bifurcation points partition the parameter space into three dynamical regimes: (I) oscillatory coexistence for $\varepsilon < \varepsilon_H$, (II) stable three-species coexistence for $\varepsilon_H < \varepsilon < \varepsilon_{BP}$ (the regime of the baseline simulation), and (III) disease-free stable coexistence for $\varepsilon > \varepsilon_{BP}$. The bifurcation structure is consistent with eco-epidemiological results in [9, 10, 20, 21].

Taken together, the results demonstrate that disease in prey, predator harvesting, and internal prey migration jointly govern the stability and long-run behavior of the ecosystem, with each factor contributing a distinct and analytically transparent mechanism. Under the baseline parameter set, the coexistence equilibrium $E_6$ is the unique locally asymptotically stable equilibrium, and its local stability is strengthened by internal migration and by sufficiently strong predation on infected prey. Whether $E_6$ is a global attractor remains an open question, as the present analysis is restricted to local stability in a neighborhood of the equilibrium.

Several directions remain open for future investigation. First, an analysis of global stability for $E_6$ using an appropriate Lyapunov function a programme carried out for related models in [21] and [10] would strengthen the local results obtained here. Second, the present model assumes a linear (Holling Type I) functional response for both prey types; extending to Holling Type II or Type III responses, as studied in [7, 8], is likely to produce richer bifurcation structures including additional Hopf points and limit-cycle branches. Third, the internal migration term $m(x_e - x)$ could be replaced by a fully spatial two-patch or reaction-diffusion formulation to capture more realistic heterogeneous habitats, following the approach of Kant and Kumar [17] and Dai et al. [18]. Finally, a rigorous analytical derivation of the first Lyapunov coefficient and formal verification of the transversality condition at $\varepsilon_H$ would confirm whether the Hopf bifurcation is supercritical or subcritical, providing a complete analytical counterpart to the numerical evidence presented here [5, 6, 20].

## CRediT Authorship Contribution Statement

**Muhammad Thariq Firmansyah:** Conceptualization, Methodology, Writing-Original Draft, Visualization. **Dian Savitri:** Data Curation, Formal Analysis, Project Administration, Validation

## Declaration of Generative AI and AI-assisted technologies

No generative AI or AI-assisted technologies were used during the preparation of this manuscript.

## Declaration of Competing Interest

The authors declare no competing interests.

## Funding and Acknowledgments

This research received no external funding.

## Data and Code Availability

The data and code supporting the findings of this study are available from the corresponding author upon reasonable request.

## References

[1] Mansur, Ahmad Ansar, and Fardinah. "Analisis Model Predator Prey dengan Adanya Penyakit Pada Prey dan Pemanenan Pada Predator". In: *Journal of Mathematics: Theory and Applications* 2.2 (2020), pp. 54–58. https://garuda.kemdiktisaintek.go.id/journal/view/23413.

[2] Alfred J. Lotka. *Elements of Physical Biology*. Reprinted as *Elements of Mathematical Biology*, Dover, 1956. Baltimore: Williams & Wilkins, 1925. https://archive.org/details/elementsofphysic017171mbp.

[3] Vito Volterra. "Variazioni e fluttuazioni del numero d'individui in specie animali conviventi". In: *Memorie della Reale Accademia Nazionale dei Lincei, Serie VI* 2 (1926), pp. 31–113. https://liberliber.it/autori/autori-v/vito-volterra/variazioni-e-fluttuazioni-del-numero-dindividui-in-specie-animali-conviventi/.

[4] Irham Taufiq and Denik Agustito. "Aplikasi Model Matematika Dua Predator dan Prey Terinfeksi dengan Kontrol Pestisida pada Penyebaran Hama Wereng Batang Cokelat di Kabupaten Bantul". In: *Jurnal Fourier* 8.2 (2019), pp. 65–72. DOI: 10.14421/fourier.2019.82.65-72.

[5] Aqiila Ollyana Savitri and Dian Savitri. "Stability and Bifurcation of a 3D Eco Epidemiological Predator–Prey Model with Pesticide". In: *CAUCHY – Jurnal Matematika Murni dan Aplikasi* 11.1 (2026), pp. 540–555. DOI: 10.18860/cauchy.v11i1.40676.

[6] Nabilah Meladelvia and Dian Savitri. "Dynamic Analysis of a Predator–Prey Model with Group Defense in Prey and Cooperative Hunting in Predators". In: *CAUCHY – Jurnal Matematika Murni dan Aplikasi* 11.1 (2026), pp. 266–278. DOI: 10.18860/cauchy.v11i1.40210.

[7] Ameer M. Sahi and Huda Abdul Satar. "Stability and Bifurcation of Prey–Predator Model with Disease in Prey Incorporating Anti-Predator and Hunting Cooperation". In: *Communications in Mathematical Biology and Neuroscience* 2025 (2025), p. 35. DOI: 10.28919/cmbn/9162.

[8] Alyaa Hussain Naser and Dahlia Khaled Bahlool. "Modeling Disease Dynamics in a Prey–Predator System with Competition, Fear, and Cooperative Hunting". In: *Computation* 13.11 (2025), p. 254. DOI: 10.3390/computation13110254.

[9] Oussama Lazaar and Mustapha Serhani. "Stability and optimal control of a prey–predator model with prey refuge and prey infection". In: *International Journal of Dynamics and Control* 11 (2023), pp. 1934–1951. DOI: 10.1007/s40435-022-01064-7.

[10] Assane Savadogo, Boureima Sangaré, and Hamidou Ouedraogo. "A mathematical analysis of prey–predator population dynamics in the presence of an SIS infectious disease". In: *Research in Mathematics* 9.1 (2022), p. 2020399. DOI: 10.1080/27658449.2021.2020399.

[11] Israr Ali, Hui Zhang, Guobao Zhang, Ali Turab, Li Wang, and Jun-Jiat Tiang. "Control of Predator Disease Dynamics Under Prey Refuge and Harvesting: A Fuzzy Computational Modeling Approach". In: *Mathematics* 13.21 (2025), p. 3362. DOI: 10.3390/math13213362.

[12] Rian Ade Pratama, Martha Loupatty, Hariyanto, Wahyu Caesarendra, and Wahyu Rahmaniar. "Fear and Group Defense Effect of a Holling Type IV Predator–Prey System Intraspecific Competition". In: *Emerging Science Journal* 7.2 (2023), pp. 385–395. DOI: 10.28991/ESJ-2023-07-02-06.

[13] Manoj Kumar Singh, Arushi Sharma, and Luis M. Sánchez-Ruiz. "Impact of the Allee Effect on the Dynamics of a Predator–Prey Model Exhibiting Group Defense". In: *Mathematics* 13.4 (2025), p. 633. DOI: 10.3390/math13040633.

[14] A. Al Themairi and Manar A. Alqudah. "Predator–prey model of Holling-type II with harvesting and predator in disease". In: *Italian Journal of Pure and Applied Mathematics* 43 (2020), pp. 744–753. https://ijpam.uniud.it/online_issue/202043/62%5C%20Themairi-Alqudah.pdf.

[15] Banani Roy and Sankar Kumar Roy. "Prey–predator model in drainage system with migration and harvesting". In: *Nonautonomous Dynamical Systems* 8 (2021), pp. 152–167. DOI: 10.1515/msds-2021-0131.

[16] Rajalakshmi Manoharan, Reenu Rani, and Ali Moussaoui. "Predator–prey dynamics with refuge, alternate food, and harvesting strategies in a patchy habitat". In: *Mathematical Biosciences and Engineering* 22.4 (2025), pp. 810–845. DOI: 10.3934/mbe.2025029.

[17] Shashi Kant and Vivek Kumar. "Stability analysis of predator–prey system with migrating prey and disease infection in both species". In: *Applied Mathematical Modelling* 42 (2017), pp. 509–539. DOI: 10.1016/j.apm.2016.10.003.

[18] Xiangjun Dai, Hui Jiao, Jianjun Jiao, and Qi Quan. "Survival Analysis of a Predator–Prey Model with Seasonal Migration of Prey Populations between Breeding and Non-Breeding Regions". In: *Mathematics* 11.18 (2023), p. 3838. DOI: 10.3390/math11183838.

[19] Érika Diz-Pita and M. Victoria Otero-Espinar. "Predator–Prey Models: A Review of Some Recent Advances". In: *Mathematics* 9.15 (2021), p. 1783. DOI: 10.3390/math9151783.

[20] Amit K. Pal, Anindita Bhattacharyya, Ashok Mondal, and Srishti Pal. "Qualitative analysis of an eco-epidemiological model with a role of prey and predator harvesting". In: *Zeitschrift für Naturforschung A* 77.7 (2022), pp. 629–645. DOI: 10.1515/zna-2021-0333.

[21] Abayneh Fentie Bezabih, Geremew Kenassa Edessa, and Koya Purnachandra Rao. "Eco-Epidemiological Model and Analysis of Prey–Predator System". In: *Journal of Applied Mathematics* 2021 (2021), p. 6679686. DOI: 10.1155/2021/6679686.

[22] Resmawan, Agus Suryanto, Isnani Darti, and Hasan S. Panigoro. *Dynamical Analysis of a Predator–Prey Model with Additive Allee Effect and Prey Group Defense*. Presented at The International Symposium on Biomathematics (Symomath), Depok, Indonesia, 10–12 July 2024. 2024. DOI: 10.48550/arXiv.2410.13345. arXiv: 2410.13345. https://arxiv.org/abs/2410.13345.

[23] Huisen Zhang. "Dynamics Behavior of a Predator–Prey Diffusion Model Incorporating Hunting Cooperation and Predator-Taxis". In: *Mathematics* 12.10 (2024), p. 1474. DOI: 10.3390/math12101474.